RELAP5-3D MODEL VALIDATION AND BENCHMARK EXERCISES FOR ADVANCED GAS COOLED REACTOR APPLICATIONS

A Thesis

by

EUGENE JAMES THOMAS MOORE

Submitted to the Office of Graduate Studies of
Texas A&M University
in partial fulfillment of the requirements for the degree of

MASTER OF SCIENCE

May 2006

Major Subject: Nuclear Engineering

RELAP5-3D MODEL VALIDATION AND BENCHMARK EXERCISES FOR ADVANCED GAS COOLED REACTOR APPLICATIONS

A Thesis

by

EUGENE JAMES THOMAS MOORE

Submitted to the Office of Graduate Studies of
Texas A&M University
in partial fulfillment of the requirements for the degree of

MASTER OF SCIENCE

Approved by:

Chair of Committee, Yassin A. Hassan
Committee Members, Kalyan Annamalai
William H. Marlow
Head of Department, William E. Burchill

May 2006

Major Subject: Nuclear Engineering

ABSTRACT

RELAP5-3D Model Validation and Benchmark Exercises for Advanced Gas Cooled Reactor Applications. (May 2006)

Eugene James Thomas Moore, B.S., The Ohio State University

Chair of Advisory Committee: Dr. Yassin A. Hassan

High-temperature gas-cooled reactors (HTGR) are passively safe, efficient, and economical solutions to the world's energy crisis. HTGRs are capable of generating high temperatures during normal operation, introducing design challenges related to material selection and reactor safety. Understanding heat transfer and fluid flow phenomena during normal and transient operation of HTGRs is essential to ensure the adequacy of safety features, such as the reactor cavity cooling system (RCCS). Modeling abilities of system analysis codes, used to develop an understanding of light water reactor phenomenology, need to be proven for HTGRs. RELAP5-3D v2.3.6 is used to generate two reactor plant models for a code-to-code and a code-to-experiment benchmark problem.

The code-to-code benchmark problem models the Russian VGM reactor for pressurized and depressurized pressure vessel conditions. Temperature profiles corresponding to each condition are assigned to the pressure vessel heat structure. Experiment objectives are to calculate total thermal energy transferred to the RCCS for both cases. Qualitatively, RELAP5-3D's predictions agree closely with those of other system codes such as MORECA and Thermix. RELAP5-3D predicts that 80% of thermal

energy transferred to the RCCS is radiant. Quantitatively, RELAP5-3D computes slightly higher radiant and convective heat transfer rates than other system analysis codes. Differences in convective heat transfer rate arise from the type and usage of convection models. Differences in radiant heat transfer stem from the calculation of radiation shape factors, also known as view or configuration factors. A MATLAB script employs a set of radiation shape factor correlations and applies them to the RELAP5-3D model.

This same script is used to generate radiation shape factors for the code-to-experiment benchmark problem, which uses the Japanese HTTR reactor to determine temperature along the outside of the pressure vessel. Despite lacking information on material properties, emissivities, and initial conditions, RELAP5-3D temperature trend predictions closely match those of other system codes. Compared to experimental measurements, however, RELAP5-3D cannot capture fluid behavior above the pressure vessel. While qualitatively agreeing over the pressure vessel body, RELAP5-3D predictions diverge from experimental measurements elsewhere. This difference reflects the limitations of using a system analysis code where computational fluid dynamics codes are better suited.

DEDICATION

To my parents, family, and friends for their invaluable love and support.

ACKNOWLEDGEMENTS

I would like to first thank Dr. Yassin A. Hassan for providing me the opportunity to conduct this research. His infectious enthusiasm for the subject provided me with constant encouragement throughout the last two years. I would also like to thank Dr. William Marlow from the Department of Nuclear Engineering and Dr. Kalyan Annamalai from the Department of Mechanical Engineering for serving on my committee and for providing insights into my research.

Next, I would like to thank Gary Johnsen for inviting me to Idaho National Laboratory where I was able to conduct the bulk of this research. My sincere gratitude is also extended to those at Idaho National Laboratory for their patience and kindness: Richard Riemke, Cliff Davis, James Fisher, and James Wolf.

Finally, I would like to thank my parents, Eugene and Peggy, and the rest of my family for encouraging me to return to graduate studies at Texas A&M University.

TABLE OF CONTENTS

Page

Page

LIST OF FIGURES

FIGURE Page

LIST OF TABLES

ACRONYMS

ACS	Auxiliary Cooling System
AVR	Arbeitsgemeinschaft Versuchs-Reaktor, German HTGR
CEA	French Atomic Energy Commission
HTGR	High-Temperature Gas-cooled Reactor
HTTR	High Temperature engineering Test Reactor
INET	Institute of Nuclear Energy Technology
LWR	Light Water Reactor
OKBM	Test Design Bureau for Machine Building
ORNL	Oak Ridge National Laboratory
RCCS	Reactor Cavity Cooling System
RELAP	Reactor Excursion Leak Analysis Program
VCS	Vessel Cooling System
VHTR	Very High Temperature Reactor
VGM	Russian modular-type helium cooled reactor

I. INTRODUCTION

A. Background

As the world grows increasingly industrialized, so, too, does the world's thirst for energy. Many options are currently being evaluated to generate enough electricity to meet these energy demands without harming the environment, such as coal gasification and nuclear power. Within the nuclear power option exists a variety of reactor plant types including pressurized water reactors, molten salt reactors, and gas-cooled reactors. Each of these reactors have been used in the past, but are being re-evaluated in light of advances in materials, increasing the capability to withstanding tremendous temperatures and pressures. These material advances are particularly essential to the high temperature gas-cooled reactor (HTGR), whose design features, developed over the last fifty years, make it an attractive option for hydrogen production.

In 1959, Germany began construction on the 15 MWe Arbeitsgemeinschaft Versuchs-Reaktor (AVR).[1] Coming on-line in 1967, this was the first nuclear plant to employ helium gas-cooled reactor technology.[2] The AVR contributed much to HTGR development over its 21 years of operation, recording a highest ever reactor coolant temperature of 950 ^{o}C, performing the first experimental simulation of a loss-of-coolant accident, and demonstrating inherent safety characteristics and fuel properties on which today's accident-resistant HTGR designs are based.[2,3]

These inherent safety characteristics stem from the use of graphite moderator, which has a high temperature capability, and TRISO fuel particles, which are an enhancement

---

This thesis follows the style of *Nuclear Technology.*

of the BISO particle.[3] The latter particles were used in the AVR and consisted of a UO_2 kernel coated with a porous pyrocarbon layer and two layers of dense pyrocarbon.[3] In contrast to the BISO particle, the TRISO particle includes an extra silicon carbide layer in between the two dense pyrocarbon layers to significantly improve the fuel's fission product retention capabilities.[3] Using helium as the primary system coolant adds to the inherent safety of the HTGR for two main reasons. First, helium is a single-phase noble gas with no heat transfer limits associated with phase change, such as departure from nucleate boiling or critical heat flux.[4] Second, helium is inert so it will not corrode system components nor will it become activated. Helium has a magic number of protons and neutrons making it especially stable and resistant to neutron absorption. Whereas helium gas flowed upward through the core in the AVR, however, helium gas cools a HTGR reactor core by flowing downward through coolant channels in the graphite fuel elements, exiting the core at high temperatures.

The HTGR is designed with many passive safety features to handle these high temperatures achieved during normal and transient operation. An annular core with an inner graphite reflector, for example, limits the fuel temperature during transients by absorbing and storing thermal energy.[5] The HTGR is also equipped with multiple decay heat removal paths both active and passive. The power conversion system and the shutdown cooling system act as active decay heat removal systems for the HTGR.[6] An independent passive reactor cooling system is also available, though, and acts to remove heat by conduction, convection, and radiation from the uninsulated reactor pressure vessel to the passive reactor cavity cooling system (RCCS).[6] During normal reactor

operation, too, the RCCS removes heat from the uninsulated reactor pressure vessel to prevent overheating of the cavity and cavity walls.[3]

The RCCS is designed to "remove all of the core afterheat in the unlikely case of failure or unavailability of the main and all other shutdown cooling systems."[7] This system also serves as "an ultimate heat sink, ensuring the thermal integrity of the fuel, core, vessel, and critical equipment within the reactor cavity for the entire spectrum of postulated accident sequences."[7] While specifics vary between plants, the general RCCS design comprises a system of cooling channels located on the periphery of an air-space surrounding the reactor pressure vessel. These oval cooling pipes are arranged in a slightly overlapping manner to prevent either direct radiation or hot air from reaching and potentially damaging the concrete wall.[3] The main cooling panels rise with the height of the pressure vessel and some RCCS designs include an upper and lower set of cooling panels. The heat removed by the RCCS depends on the temperature of the cooling tubes and on the temperature of the reactor pressure vessel. In most designs, the RCCS coolant is either water or air with each coolant having a set of advantages and disadvantages.

Dilling et al. evaluated the performance of natural draft air cooling and forced water cooling with a passive mode based on functions and requirements, operability, licenseability, and cost.[8] The study found the air cooling system preferable to the water cooling system because it is more passive and, because of its simpler design, has less failure modes.[8] In contrast, forced water cooling has complexities related to switching between active and passive modes of operation and to two-phase flow, which may occur as the water inside the tubes begins to boil.[8] A water-cooled RCCS would also be much

heavier than air-cooled RCCS. The study concluded that with the increased cost due to these complexities, the air-cooled RCCS is more attractive than the water-cooled RCCS.[8]

The Very High Temperature Reactor (VHTR) is a Next Generation Nuclear Plant that builds on the HTGR design, incorporating the RCCS and other safety features. The VHTR achieves higher temperatures than the HTGR, however, which poses problems for the selection of reactor plant materials. Computational analysis is required to show that material temperature limits are not exceeded during normal operation or during accidents. Furthermore, interactions between the reactor and the balance of plant necessitate a system-wide analysis.[5] Detailed understanding of the physical phenomena of the RCCS such as the heat transfer and the flow behavior during normal and transient operations are important to ensure the adequacy of the RCCS. Systems analysis codes, such as RELAP5-3D, are suited to this task but, while the basic physical models have been proven for light water reactors, the application of these models to HTGR and NGNP designs must be validated.

B. Objectives

The report IAEA-TECDOC-1163, titled "Heat Transport and Afterheat Removal for Gas Cooled Reactors under Accident Conditions," is a compilation of different code-to-code and code-to-experiment benchmark evaluations related to the RCCS.[7] The objective of the present study is to simulate two selected benchmark exercises to assess the performance of the RELAP-3D thermal hydraulic system computer program. Version 2.3.6 of the code is used in the assessment of the two models that compares the RELAP5 code predictions against available experimental or other codes' results.

The first benchmark exercise is a code-to-code benchmark using a Russian VGM RCCS mockup and the second benchmark exercise is a code-to-experiment benchmark using a Japanese High Temperature Engineering Test Reactor (HTTR) RCCS mockup. The VGM and HTTR reactors and experimental setups are described in Sections II and III, respectively. A brief review of RELAP5-3D v2.3.6 computer program and its various features is presented in Section IV. Nodalization schemes for the two reactors are presented in Section V. The simulation results are presented in Section VI and conclusions of the present study are summarized in Section VII.

II. MODULAR-TYPE HELIUM COOLED REACTOR (VGM)

A. Background

The VGM is the third in a series of HTGRs developed in Russia starting in 1963. The second project in the series, the 1060 MW thermal power (MWt) VG400 reactor, began in 1974 for producing both electricity and process heat.[3] The heat from the VG400 was transferred to a methane steam reformer where hydrogen was gained for ammonia production.[9] Two different core designs, using a pebble bed and a prismatic fuel, were tested with the reactor. However, the Russians found that manufacturing and refueling using fuel pellets required more simple technology relative to prismatic fuel. This, coupled with the capability to refuel while the reactor was running, led the Russians to select the pebble bed design for further development. Incorporating these lessons, the next reactor project in the series, the 200 MWt VGM reactor, began in 1986. A modular type-high temperature helium cooled reactor, the VGM was developed to "validate main technical decisions associated with production of high temperature process heat."[9]

The main reactor plant parameters are shown in Table I. A side view of the VGM with a list of the main equipment can be found in Fig. 1. The lower part of the vessel, approximately 6 m high, is covered with insulation of 100 mm thickness. Air at atmospheric pressure fills the space between the cylindrical reactor vessel and the 432 cooling channels, arranged into three independent units of 144 tubes each. These units have their own inlet and outlet manifolds. A reflective screen surrounds the cooling tubes. The arrangement of the RCCS is shown as a side view in Fig. 2 and as a plan view in Fig. 3.

TABLE I

Main characteristics of the VGM reactor plant

PARAMETER	VALUE
Thermal power, MWt	200
Helium temperature, C	
reactor inlet	300
reactor outlet	750…950
Helium flow rate, kg/s	59…85
Helium pressure, Mpa	5
Number of loops	1 main and 1 auxiliary

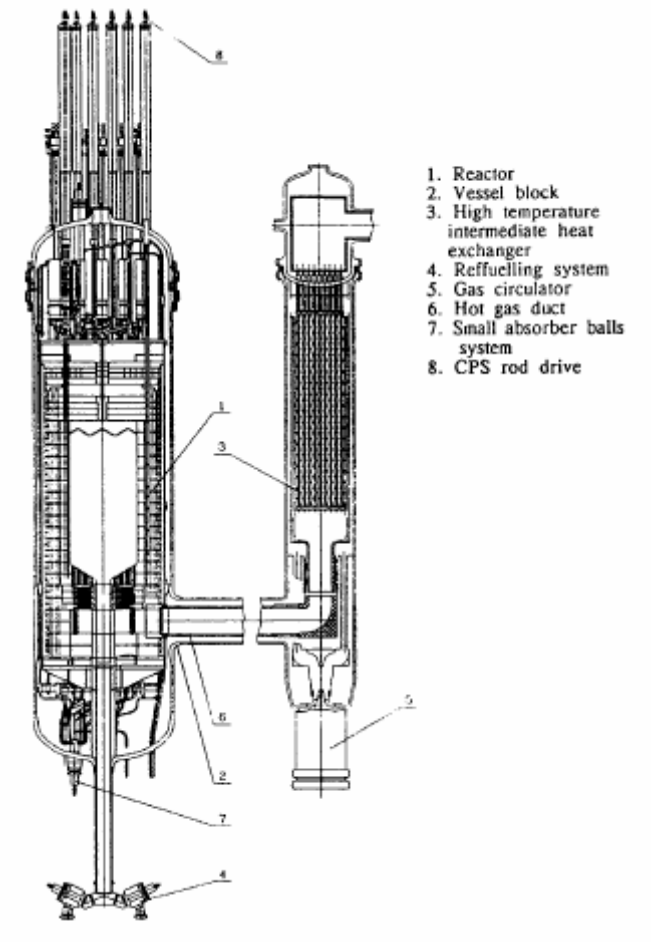

Fig. 1. VGM reactor plant.

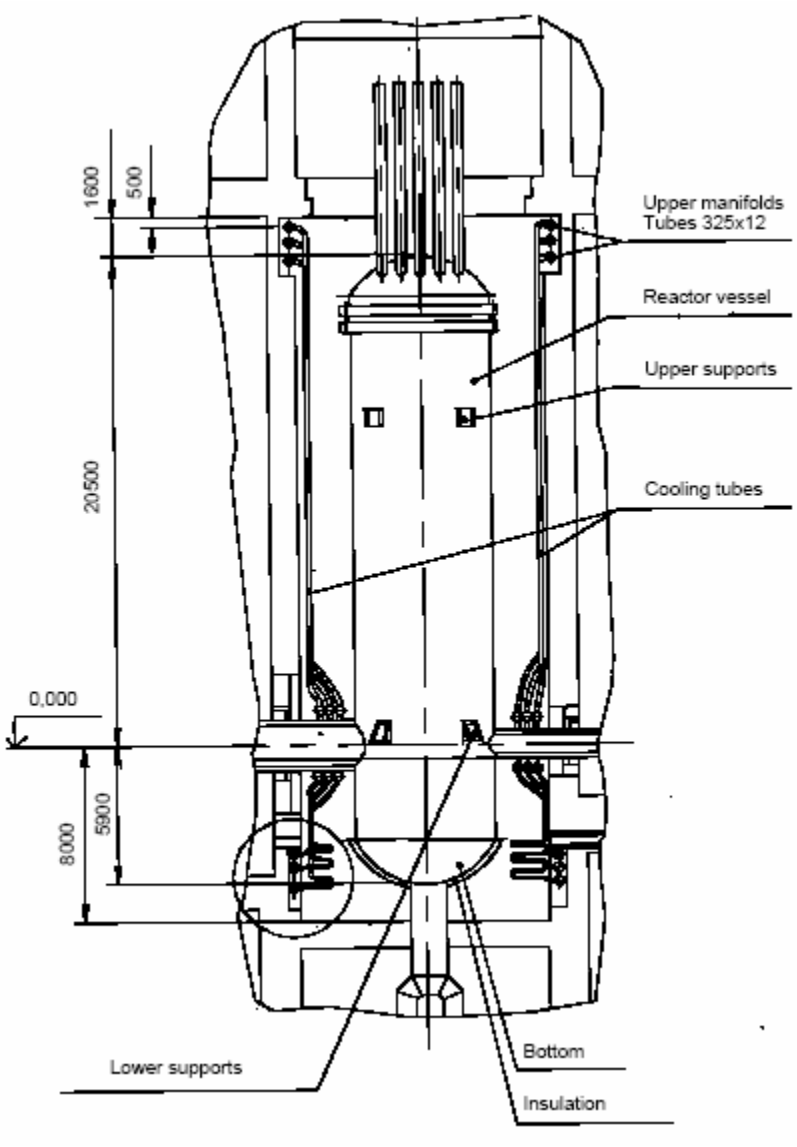

Fig. 2. Arrangement of the reactor cavity cooling system.

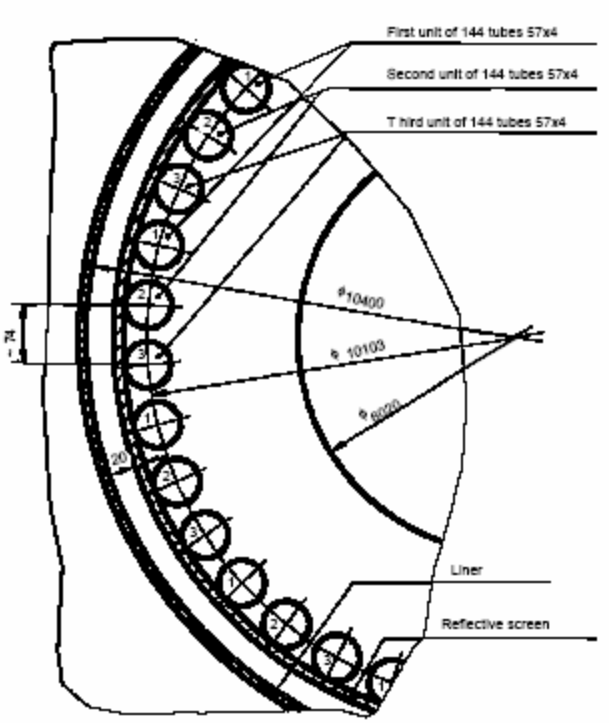

Fig. 3. Reactor cavity cooling system.[7]

B. Benchmark Problem

The benchmark exercise is a code-to-code benchmark using a VGM RCCS mockup. The objective of the benchmark exercise for this model is to calculate total thermal energy transferred from the reactor vessel to the RCCS by radiation and convection for a pressurized and depressurized heatup accident.[7] For each case, a different reactor vessel temperature profile is given, which is used as the driving boundary condition. Fig. 4 shows this reactor pressure vessel temperature profile for both cases. The important RCCS parameters, such as temperature and flow rate, are tabulated in Table II. Those reporting results to this code-to-code benchmark include the Institute of Nuclear Energy Technology (China), OKBM (Russian Federation), and Oak Ridge National Laboratory (USA).

OKBM uses two codes: DUPT and SM1. The former is a two-dimensional code used in modeling temperature and velocity distributions in gas cavities.[7] An important note about the two-dimensional SM1 code is that it does not compute fluid flow, instead modeling heat transfer by fluids through boundary conditions.[7] In the radiation model of SM1, the interacting surfaces are assumed to be at right angles to each other, ignoring an angular distribution of radiant heat.[7] MORECA, used by ORNL, simulates accident scenarios for certain gas-cooled reactor types.[7] INET conducts their analysis using Thermix, which performs two-dimensional thermal hydraulic analyses of operating and accident conditions.

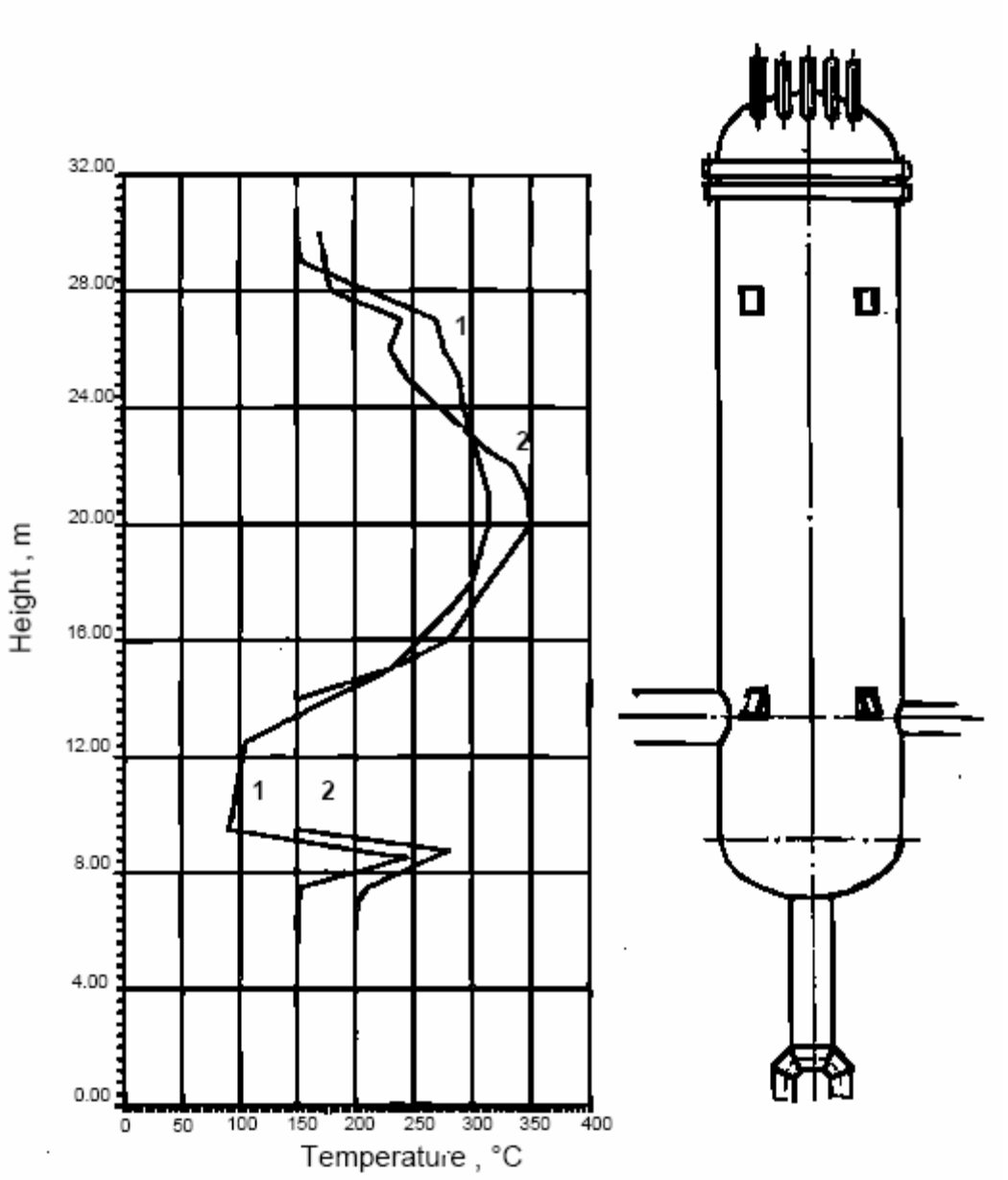

Fig. 4. Temperature distribution on the height of the reactor vessel.[7]
1- pressurized conditions
2- depressurized conditions

TABLE II

Data for calculation

Parameter	Value
Accident conditions (pressurized)	
Temperature of water at inlet of the RCCS, °C	43
Flowrate of water through three units, kg/s	29.46
Helium pressure in the plenum between the plate and the upper head, MPa	4.9
Emissivity of the pressure vessel	0.8
Emissivity of the surface cooler	0.8
Accident conditions (depressurized)	
Temperature of water at inlet of the RCCS, °C	42
Flowrate of water through three units, kg/s	30.9
Helium pressure in the plenum between the plate and the upper head, MPa	0.1
Emissivity of the pressure vessel	0.8
Emissivity of the surface cooler	0.8

III. HIGH TEMPERATURE ENGINEERING TEST REACTOR (HTTR)

A. Background

The goal of the HTTR project, Japan's first HTGR, is to establish and upgrade the HTGR technological basis. Construction began in 1991 and ten years later, on December 7, 2001, the HTTR achieved its first full power of 30MWt at rated operation.[10] Because the HTTR is a test reactor being used not only to advance HTGR knowledge but also to provide irradiation spaces for research in high temperature engineering, the reactor core uses a pin-in-block type of fuel rather than a pebble bed.[11] The reason for this choice is that high temperatures can more easily be achieved using the block type fuel than in the pebble bed.[11]

The main reactor plant parameters can be found in Table III. The passive or inherent safety design of the HTTR is standard with respect to other current HTGR designs. The reactor cooling system, shown in Fig. 5, is composed of a main cooling system, an auxiliary cooling system (ACS), and a vessel cooling system (VCS).[11] The main cooling system consists of primary and secondary helium cooling systems and a pressurized water cooling system. The ACS is an engineering safeguard designed to cool the core and metallic components upon a reactor scram. The VCS is the RCCS, acting to cool the concrete containment and to remove the decay heat and excess heat from the reactor pressure vessel.

TABLE III

Major specifications of the HTTR[11]

Thermal power	30MW
Outlet coolant temperature	850°C/950°C
Inlet coolant temperature	395°C
Fuel	Low enriched UO_2
Fuel element type	Prismatic block
Direction of coolant flow	Downward
Pressure vessel	Steel
Number of cooling loop	1
Heat removal	IHX and PWC (parallel loaded)
Primary coolant pressure	4MPa
Containment type	Steel containment
Plant lifetime	20 years

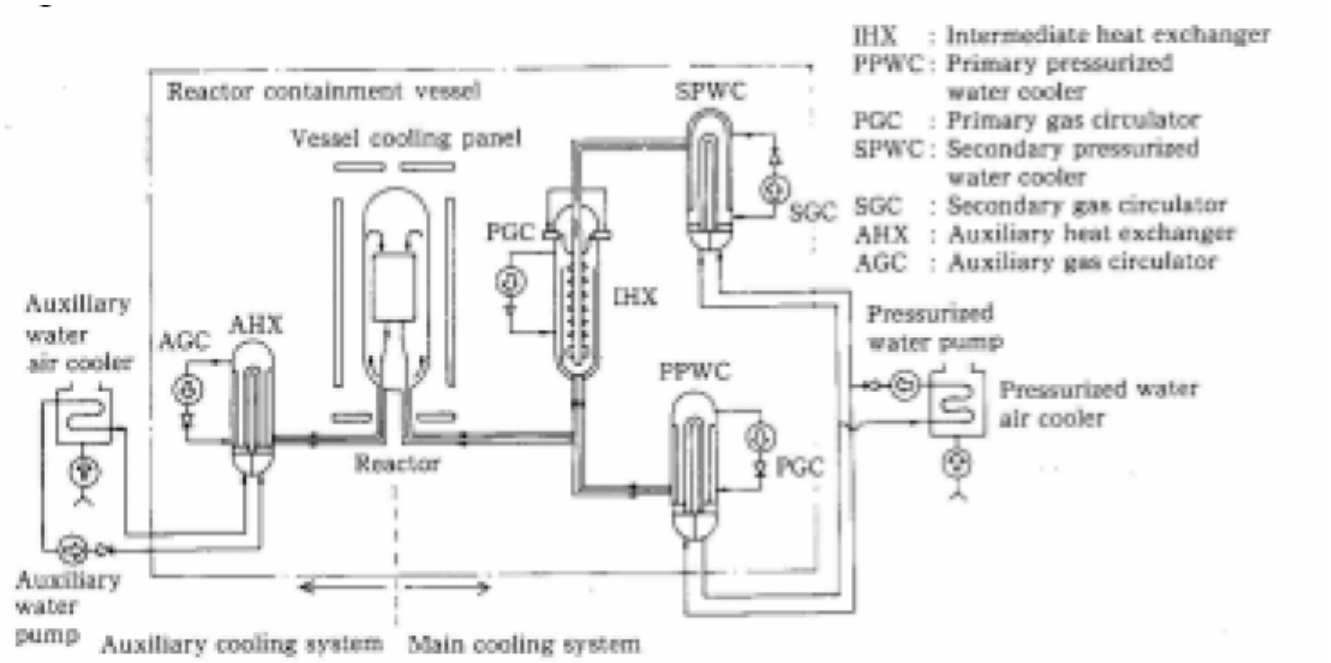

Fig. 5. Cooling system of the HTTR.[11]

B. Benchmark Problem

The benchmark exercise is a code-to-experiment benchmark using a HTTR RCCS mockup. A comparison of the main features of the mockup to their HTTR VCS counterparts is shown in Table IV. Fig. 6 shows the flowpath of the test setup, which consists of a test section with systems to supply water and helium gas or to create a vacuum. A two-dimensional schematic of the test section that displays the RCCS is shown in Fig. 7. The three-dimensional schematic of Fig. 8 more clearly shows the arrangement of the support legs and the location of the sheathed chromel-alumel thermocouples.

TABLE IV

Comparison of the HTTR VCS system with the experimental apparatus[7]

Item	Present apparatus	HTTR
Pressure Vessel		
Height / Diameter	3 m / 1m	13.2m / 5.7m
Temperature	450 C	450 C
Reactor Core (Heater)		
Height / Diameter	2 m / 0.6 m	8 m / 4.3 m
Temperature	600C	860C
Heat Flux (of Decay Heat)	25kW/m^2	17.5kW/m^2
Total Heat (of Decay Heat)	100kW	2400kW
Water Cooling Panel		
Height / Width	3.4m / 2.9m	14.7 m / 8.5 m
Pitch of water tube	60 mm	60 mm
Flow rate of water	10 t/h	90 t/h

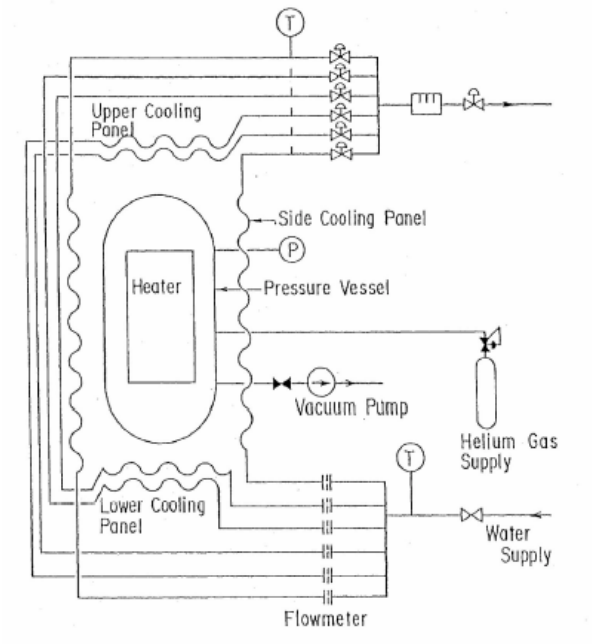

Fig. 6. Schematic of test apparatus.[7]

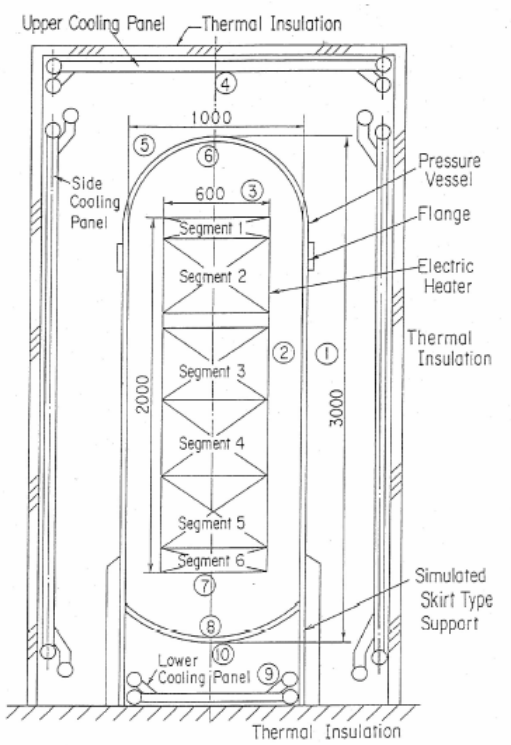

Fig. 7. Schematic of pressure vessel and RCCS.[7]

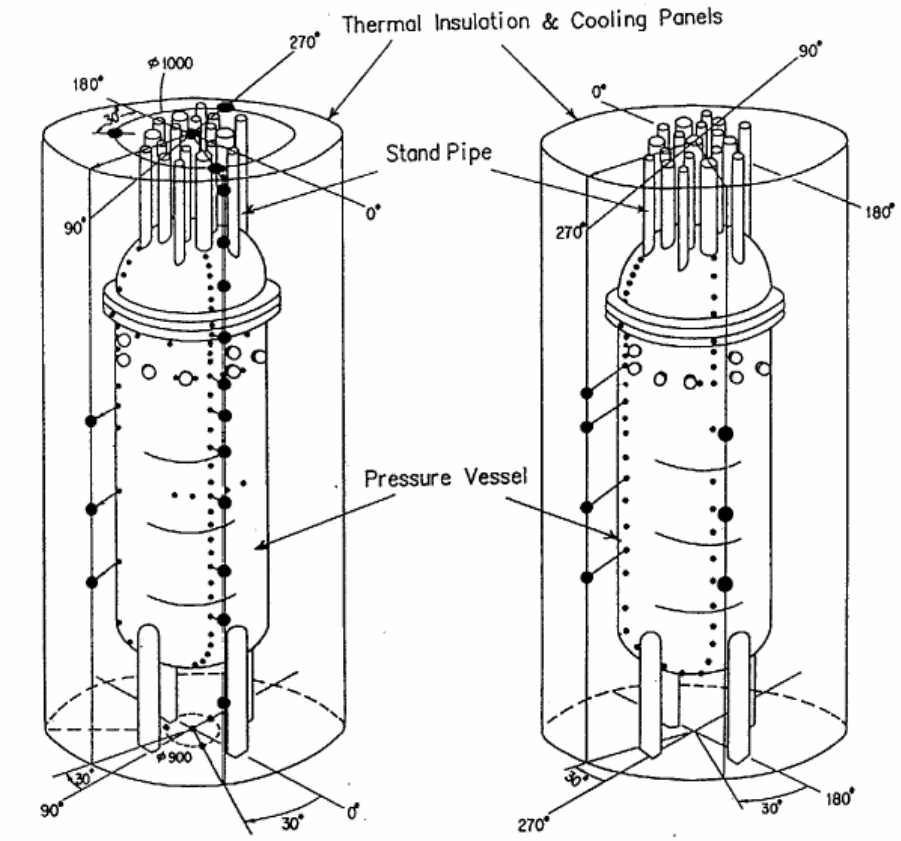

Fig. 8. Measuring points of temperatures in the test section.[12]

The reactor pressure vessel in the mockup is made from stainless steel and has 19 stainless steel standpipes located on the top and a plain carbon steel support skirt surrounding the vessel base. These standpipes are removable, but, when installed, act to prevent heat transfer by convection or radiation through the top of the pressure vessel. The mockup replaces the reactor core with six segments of electric heaters installed vertically inside the pressure vessel. These heaters are comprised of a wire-bound ceramic block. The cooling panel surrounds the pressure vessel and removes heat from the heaters by radiation and convection of the gas inside the pressure vessel and the air outside the pressure vessel. The cooling panel has an upper, lower, and side section as shown in Fig. 7. Black paint coats both the cooling panel and the reactor pressure vessel

to create a constant emissivity in the air-space. Thermal insulation encircles the test setup, including the cooling panel, to minimize external effects.

Seven different experiments are performed, varying the type of gas inside the pressure vessel between helium and nitrogen, the pressure of this gas, the heat input profile from the heating segments, the cooling channel fluid, and the presence of standpipes on the pressure vessel. The experiment parameters are tabulated in Table V. The six heater segments have heat transfer areas described in Table VI. Temperatures of the heaters, the pressure vessel, and the side cooling panels are measured for these experiments. However, most of the reported results for this exercise use the temperature distribution on the exterior of the pressure vessel as the point of comparison between computational and experimental results. In the RELAP5-3D analysis, the temperature measured along the surface of the RCCS is used as another input parameter. Some of those reporting results for this benchmark include the CEA (France), JAERI (Japan), INET (China), OKBM (Russia), and ORNL (USA).

The CEA simulates the benchmark experiments using TRIO-EF CASTEM 2000, which is a 3D flow, conduction and radiation heat transfer code.[7] JAERI conducts their analyses using Thermix while OKBM uses DUPT and SM1 codes. MORECA is used by ORNL.

TABLE V

Detailed conditions of the experiments[7]

Benchmark Problem	(I)	(II)	(III)	(IV)	(V)	(VI)-a	(VI)-b
Item of gas		He	N_2	He	He	He	He
Pressure(MPa)	$1.3x10^{-6}$	0.73	1.1	0.47	0.64	0.96	0.98
Heat input							
Total input(kW)	13.14	28.79	93.93	77.54	29.71	2.58	7.99
heater segment							
No.1 (kW)	1.01	1.16	5.90	5.63	1.80	0	0
No.2	2.31	3.11	16.05	19.60	5.23	0	0
No.3	2.64	3.52	19.88	21.59	5.68	0	0
No.4	2.46	5.10	22.24	22.70	11.26	0	0
No.5	3.76	10.42	22.13	0	0	0	0
No.6	0.96	5.49	7.72	8.00	5.74	2.58	7.99
Cooling panel	Water	Water	Water	Water	Air	Air	Air
Stand pipes	No	No	No	With	With	With	With

TABLE VI

Heat transfer area of heater segments[7]

Heater Segment	Heat Transfer Area, m^2
1	0.283
2-5	0.848
1	0.135

IV. RELAP5-3D COMPUTER PROGRAM

Around 1976, Idaho National Laboratory began development on a reactor excursion leak analysis program, or RELAP. This code used a card-based input deck and was designed to simulate transients in light water reactors (LWR) including, but not limited to, a loss of coolant accident or a station blackout. In the thirty years since, the code has been continuously improved, incorporating new models and refining existing models. RELAP5-3D, the most recent in the series, adds a multi-dimensional thermal hydraulic and kinetic modeling capability. RELAP5-3D is a "highly generic code that, in addition to calculating the behavior of a reactor coolant system during a transient, can be used for simulation of a wide variety of hydraulic and thermal transients in both nuclear and nonnuclear systems involving mixtures of vapor, liquid, noncondensable gases, and nonvolatile solute."[13] Version 2.3.6 of the RELAP5-3D code will be used in the assessment of the two models. The details presented in this chapter have been obtained from available references on RELAP.[13] This chapter highlights a few details of the hydrodynamic and heat structure models that pertain to the benchmark experiments and briefly discusses some important points related to problem modeling.

A. Hydrodynamic Model

The hydrodynamic model is a transient, two-fluid and two-phase flow model. While its predecessors used a one-dimensional model for the transient flow, RELAP5-3D is capable of modeling transient multi-dimensional flow. RELAP5-3D also uses a nonhomogeneous, nonequilibrium two-phase flow model, but options exist for using homogeneous, equilibrium model instead. The two-phase model encompasses a

vapor/gas-liquid mixture but the vapor/gas phase may contain a noncondensable component and the liquid phase may contain a nonvolatile solute. For the two-fluid, nonequilibrium model, the phasic continuity, momentum, and energy equations form the basic field equations. The basic, two-phase, single-component model can be extended to account for the presence of a noncondensable component in the vapor/gas phase, by assuming that the noncondensable component flows with same velocity and temperature as the vapor phase.

The two-fluid equations of motion use volume and time-averaged parameters of the flow. The constitutive models used for defining flow regimes and related models such as wall friction, wall heat transfer, and interphase mass and heat transfer, are based on experiments in terms of average or macroscale parameters. These are important points to consider when selecting node sizes because if the nodes are made too small, these models may not apply. Therefore, the ratio of the node length to node diameter should be unity or greater. This restriction will be called the length-diameter restriction. In addition to this lower bound for node sizes, there is an upper bound defined by where, if the nodes are too large, the spatial convergence of the results is compromised. Nodalization sensitivity studies are thus conducted in the benchmark simulations.

The RELAP5-3D simulation program solves eight field conservation equations for eight primary dependent variables: pressure, phasic internal energies, volume vapor void fraction, phasic velocities, noncondensable quality, and boron density. Secondary dependent variables are phasic densities, phasic temperature, saturation temperature, and noncondensable species mass fraction in the noncondensable gas phase. The independent variables are time and distance, which can be one-dimensional or three-dimensional.

Internal flow in pipes forms the basis for wall heat transfer correlations. Convection equations evaluate correlations by Dittus-Boelter, Kays, and Churchill-Chu that deal with forced turbulent convection, forced laminar convection, and natural convection, respectively. RELAP5-3D then selects the maximum of these evaluations for use in the component model.

RELAP5-3D contains a variety of component models which are used to build system models. For example, in the VGM model, pipe and annulus components are used to model the air-space between the pressure vessel and the RCCS and the water flowing through the RCCS. Both pipe and annulus component are a series of volumes connected by interior junctions, where the outlet of one volume feeds through the junction into the inlet of another volume. The two component models are identical except in modeling of the annular-mist flow regime. In the annulus component, all the liquid is in the film with no liquid entrained in the vapor when the flow regime is annular-mist. Furthermore, the annulus component should be only used to model a vertical annular region. These hydrodynamic components are coupled to heat structures representing the various pipe, tube, or vessel walls.

B. Heat Structure Model

A heat structure represents the solid portion of the thermal-hydraulic system. Heat structures play an important role in a system-wide analysis as system response depends on heat transfer between the heat structures and the fluid. Temperature dependent material properties, such as thermal conductivity and volumetric heat capacity, can be specified either by a table or by a set of functions. Initial heat structure

temperatures are assigned as a starting point for iterations on temperature-dependent thermal properties and boundary conditions.

Heat structure temperature distribution and heat transfer rates are calculated by the transient heat conduction equation for rectangular, cylindrical, or spherical geometry. Mesh points are numbered from left to right in each geometry, which is insignificant for surfaces in a rectangular geometry. In cylindrical or spherical geometry, however, the left and right surfaces represent the inner and outer diameters, respectively. Each side may be connected to a hydrodynamic volume. Each heat structure surface can only participate in one enclosure, whether conduction or radiation. This is a significant point for the benchmark experiments, which assumes that radiant effects on the heat structure are dominant over conduction effects within the heat structure. Participation in an enclosure, however, still permits the application of a convective boundary condition.

1. Radiation Enclosure Model

The radiation enclosure model calculates heat transfer directly between heat structures using a lumped-system approximation for gray diffuse surfaces contained in an enclosure. This model assumes that, first; fluid in the void-space between the heat structures neither absorbs nor emits radiant thermal energy, second; reflectance from a surface is independent of incident or reflected direction and of radiation frequency, and third; radiant properties such as temperature, reflectance, and radiosity are constant over each surface. The radiosity, R_i, of a surface is the radiant energy flux leaving that surface and is defined by Eq. (1)

$$R_i = (\delta_{ij} - \rho_i F_{ij})^{-1} \varepsilon_i \sigma T_i^4 , \tag{1}$$

where

δ_{ij} = 0 for i ≠ j

δ_{ij} = 1 for i = j

ε = emissivity

ρ = (1-ε); reflectivity

σ = Stefan-Boltzmann constant

T = temperature

F_{ij} = view factor from surface i to surface j.

Using this definition for radiosity, the net heat flux, Q_i, at surface i is then given by Eq. (2).

$$Q_i = \frac{\varepsilon_i}{\rho_i}(\sigma T_i^4 - R_i), \tag{2}$$

The heat conduction equation for the i-th surface is found in Eq. (3)

$$-k\left.\frac{\partial T}{\partial n}\right|_i = h_i(T_i - T_{sk}) + Q_i, \tag{3}$$

where

k = surface conductivity

n = unit normal vector away from the boundary surface

h = convective heat transfer coefficient

T_{sk} = sink temperature.

View factors can be calculated in a variety of ways, using mechanical, integral, or graphical methods. Also known as configuration or shape factor, the view factor between two surfaces, 1 and 2, represents the fraction of radiant thermal energy that leaves surface 1 and reaches surface 2. These view factors are subject to two principles represented in

Eq. (4), the reciprocity rule, and Eq. (5), the summation rule, which says that the sum of all the fractions has to equal 1.0.

$$A_1 F_{12} = A_2 F_{21}, \tag{4}$$

$$\sum_{j}^{no.\_cells} F_{i-j} = 1.0, \tag{5}$$

RELAP5-3D checks the view factors entered in the input deck against Eq. (4) and Eq. (5) to ensure satisfaction within 0.1 percent. This requirement prevents energy conservation errors from becoming too large.

C. Problem Modeling

For both VGM and HTTR benchmark problems, simulations are run to steady state. In RELAP5-3D, this means that time-average steady-state is achieved when the mean rate of change in system enthalpy is within certain limits. In the hydrodynamic solution scheme, the following three terms are monitored whose variation in time includes the variation of all the other terms: thermodynamic density, internal energy, and pressure. Since enthalpy is the sum of the internal energy plus the product of pressure and volume, monitoring the time variation of enthalpy is equivalent to monitoring the time variation of all the other variables in the solution scheme.

V. NODALIZATION SCHEME

A RELAP5-3D input deck is built for each model and each associated experiment. This section details the nodalization process for the benchmark experiments, which is essentially the same in both cases. Aspects of nodalization common to both models are discussed first. A discussion on the shape factor calculation is then presented, followed by a summary of nodalization details specific to each model.

Building the RELAP5-3D input deck entails some simplification of the model geometry including discretizing the domed top and bottom of the pressure vessel into a series of stacked cylinders and modeling the multitude of RCCS cooling channels as a single outer annulus. RELAP5-3D assumes azimuthal symmetry so some piping and support structures are not modeled. Further model simplification involves the side cooling panels seen in Fig. 2 and Fig. 7, which bend into the air-space at the top and bottom of the panel. In the RELAP5-3D model, these bends are flattened, making an outer annulus of constant radius. The length-diameter restriction sets the lower bound for the number of nodes. The number of nodes within a radiation enclosure is limited to 99, which sets the upper bound for the number of nodes.

A MATLAB script aids in creating the input deck. This script reads model parameters such as temperature or power profile and model dimensions and creates a nodal model complete with shape factors and nodal areas, volumes, heights, and hydraulic diameters. The script then presents this information in a format easily copied into the RELAP5-3D input deck. The main function of the script, however, is to calculate shape factors between heat structure surfaces precisely enough to satisfy the reciprocity and summation checks performed by RELAP5-3D. The shape factor

calculation in the MATLAB script employs a series of correlations developed by Dr. John Howell of University of Texas.[14] Hottel's crossed-string method of evaluating shape factors was also considered but was rejected as the method applies only to two-dimensional geometries.[15] The contour integration method of determining shape factors was rejected because the computation is not suited to handling obstructions, such as in the shape factor calculation from a cell below the pressure vessel to a cell above the pressure vessel.[15] Paying extra attention to the radiation heat transfer is warranted because benchmark results show, particularly in the VGM model, that radiant heat transfer constitutes approximately 75% of the total heat transfer to the cooling channel.[7]

A. Radiation Shape Factor Calculation

Dr. John Howell from the University of Texas maintains a catalog of shape factors correlations for three different scenarios: a differential area to a differential area, a differential area to a finite area, and a finite area to a finite area. Three of these correlations, which are well suited for computational work, are selected for the benchmark analysis. It is important to reiterate that within RELAP5-3D's radiation enclosure model, the shape factors are input for left and right surfaces only, complicating the discretization process. These correlations and their governing equations are fully described below with an accompanying figure which more clearly shows the correlation's intended use. Following these descriptions is a discussion on how the MATLAB script uses these correlations together.

1. Shape Factor Correlation C-92

Given concentric right circular cylinders of equal finite length represented in Fig. 9, this correlation calculates the shape factor from the interior surface of the outer cylinder to the exterior surface of the inner cylinder. [14]

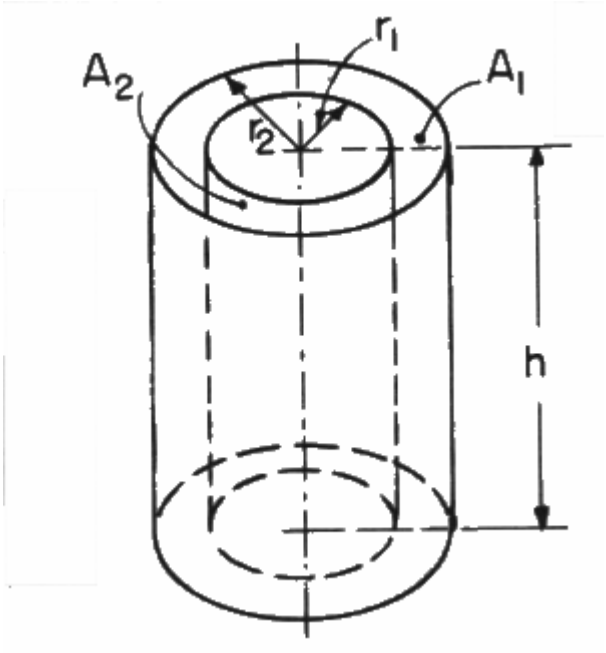

Fig. 9. Surfaces used with the C-92 shape factor correlation. [14]

C-92's governing equation is shown in Eq. (6)

$$F_{1-2} = \frac{1}{\pi R_2}\left\{\begin{array}{l}\frac{1}{2}\left(R_2^2 - R_1^2 - 1\right)\cos^{-1}\left(\frac{R_1}{R_2}\right) + \pi R_1 - \frac{\pi}{2}AB - 2R_1\tan^{-1}\left(R_2^2 - R_1^2\right)^{\frac{1}{2}} \\ + \left[\left(1+A^2\right)\left(1+B^2\right)\right]^{\frac{1}{2}}\tan^{-1}\left[\frac{\left(1+A^2\right)B}{\left(1+B^2\right)A}\right]\end{array}\right\}, \qquad (6)$$

where $R_1 = \frac{r_1}{h}$; $R_2 = \frac{r_2}{h}$; $A = R_2 + R_1$; $B = R_2 - R_1$.

2. Shape Factor Correlation C-95

Given concentric right circular cylinders of finite length represented in Fig. 10, where the interior cylinder is completely inside the exterior cylinder, this correlation calculates the shape factor from the exterior surface of the inner cylinder to the interior surface of the outer cylinder.

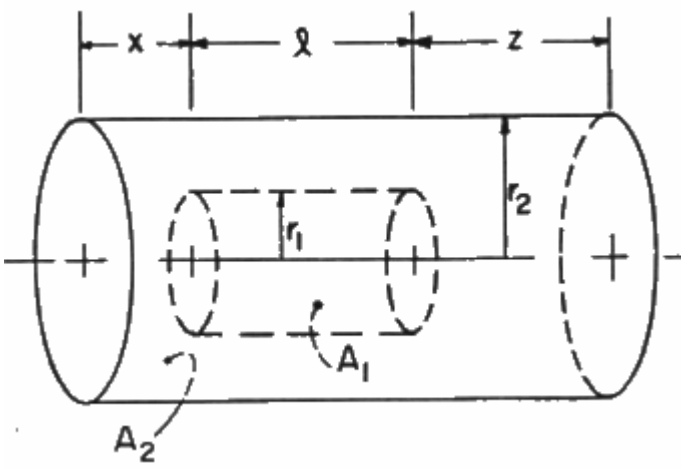

Fig. 10. Surfaces used with the C-95 shape factor correlation. [14]

C-95's governing equation is shown in Eq. (7)

$$F_{1-2} = 1 + \frac{X}{L} F_X + \frac{Z}{L} F_Z - \left(\frac{L+X}{L} \right) F_{L+X} - \left(\frac{L+Z}{L} \right) F_{L+Z}, \tag{7}$$

where $X = \frac{x}{r_2}$; $Z = \frac{z}{r_2}$; $L = \frac{l}{r_2}$; $R = \frac{r_1}{r_2}$; $A_\xi = \zeta^2 + R^2 - 1$; $B_\xi = \zeta^2 - R^2 + 1$;

$$F_\xi = \frac{B_\xi}{8R\xi} + \frac{1}{2\pi} \left\{ \cos^{-1}\left(\frac{A_\xi}{B_\xi} \right) - \frac{1}{2\xi} \left[\frac{\left(A_\xi + 2\right)^2}{R^2} - 4 \right]^{\frac{1}{2}} \cos^{-1}\left(\frac{A_\xi R}{B_\xi} \right) - \frac{A_\xi}{2\xi R} \sin^{-1} R \right\}.$$

3. Shape Factor Correlation C-101

Given parallel opposed cylinders of unequal radius and equal finite length represented in Fig. 11, this correlation calculates the shape factor from cylinder 1 to cylinder 2.

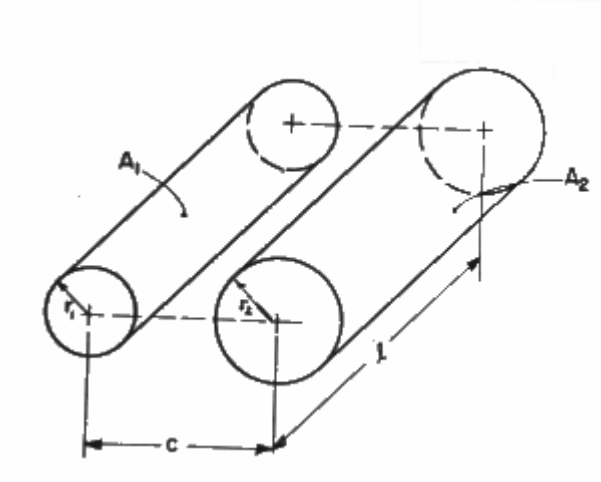

Fig. 11. Surfaces used with the C-101 shape factor correlation. [14]

C-101's governing equations are shown in Eq. (8) through Eq. (12)

$$A=\frac{1}{2\pi R}\left\{\begin{array}{l}\left[C^2-(1+R)^2\right]^{\frac{1}{2}}-\left[C^2-(1-R)^2\right]^{\frac{1}{2}}+\pi R+(1-R)\cos^{-1}\left(\frac{1-R}{C}\right)\\-(1+R)\cos^{-1}\left(\frac{1+R}{C}\right)\end{array}\right\}, \quad (8)$$

$$B=\frac{1}{\pi}\sin^{-1}\left(\frac{1}{C}\right), \quad (9)$$

$$C=1-\frac{1}{\pi}\left(\cos^{-1}\left(\frac{Y_1}{Z_1}\right)-\frac{1}{2RL}\left\{\begin{array}{l}\left[\left(Y_1+2X_1^2\right)^2-\left(2X_1R\right)^2\right]^{\frac{1}{2}}\cos^{-1}\left(\frac{RY_1}{X_1Z_1}\right)\\+Y_1\sin^{-1}\left(\frac{R}{X_1}\right)-\frac{\pi}{2}Z_1\end{array}\right\}\right), \quad (10)$$

$$D = 1 - \frac{1}{\pi}\left(\cos^{-1}\left(\frac{Y_2}{Z_2}\right) - \frac{1}{2L}\left\{ \begin{array}{l} \left[\left(Y_2 R^4 + 2X_2^2\right)^2 - \left(2X_2\right)^2\right]^{\frac{1}{2}} \cos^{-1}\left(\dfrac{Y_2}{X_2 Z_2}\right) \\ + R^2 Y_2 \sin^{-1} X_2 - \left(\dfrac{\pi R^2 Z_2}{2}\right) \end{array} \right\} \right), \quad (11)$$

$$E = 1 - \frac{1}{\pi}\cos^{-1}\left(\frac{L^2 - X^2}{L^2 + X^2}\right), \quad (12)$$

where $R = \frac{r_1}{r_2}$; $L = \frac{l}{r_2}$; $C = \frac{c}{r_2}$;

$$X_1 = \left[\frac{\left(C_2 - 1\right)^{\frac{1}{2}} - \left(\frac{\pi}{2}\right)}{\sin^{-1}\left(\frac{1}{C}\right)} + 1 \right]^{\frac{1}{2}}; \; X_2 = R\left\{ \frac{\left[\left(\frac{C}{R}\right)^2 - 1\right]^{\frac{1}{2}} - \frac{\pi}{2}}{\sin^{-1}\left(\frac{R}{C}\right)} + 1 \right\}^{\frac{1}{2}};$$

$Y = L^2 - X^2 + R^2$; $Z = L^2 + X^2 - R^2$.

Equations (8) through (12) are used with Table VII to find the shape factor from cylinder 1 to cylinder 2.

TABLE VII

C-101 tabulated values obtained by numerical integration[14]

R	L	(C-R-1)= 0.0	0.5	1.0	2.0
0	0.5	0.500	0.1037	0.0446	
	1.0		0.1526	0.0772	
	5.0				
	10.0		F12 = B x E		
	50.0				
0.1	0.5	0.3453	0.0933	0.0415	
	1.0		0.1387	0.0721	
	5.0				
	10.0		F12 = A x C		
	50.0				
1	0.5	0.1440	0.0517	0.0264	
	1.0				
	5.0		F12 = A x C		
	10.0	0.1813			
	50.0	0.1834			
10	0.5	0.0233	0.0104	0.0062	0.0032
	1.0	0.0276	0.0167	0.0111	0.0062
	5.0	0.0344	0.0288	0.0246	0.0186
	10.0		F12 = A x D		0.0229
	50.0				

4. Shape Factor Correlation B-55

Given concentric right circular cylinders of equal finite length represented in Fig. 12, this correlation calculates the shape factor from an element at the end of the outer cylinder to the interior surface of the outer cylinder.

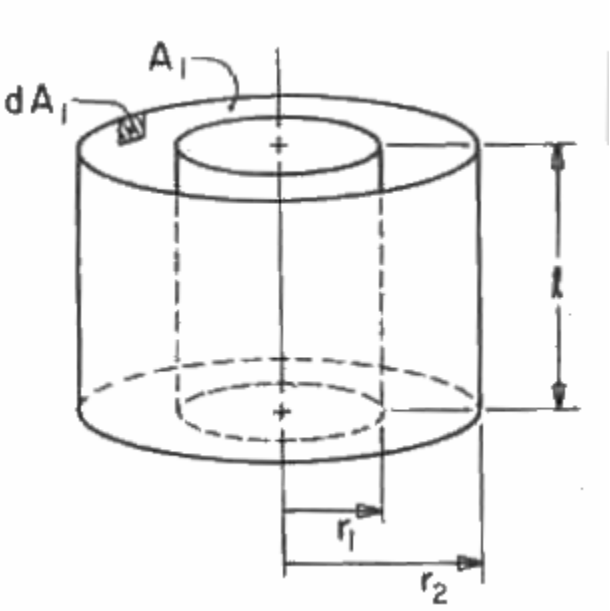

Fig. 12. Surfaces used with the B-55 shape factor correlation.[14]

B-55's governing equation is shown in Eq. (13)

$$F_{d1-2} = \frac{1}{2} - \frac{1}{4R} + \frac{1}{\pi R}\left\{\begin{array}{l} L\tan^{-1} X - \frac{1}{2}\tan^{-1}\left(\frac{L^2 - 4X^2}{4LX}\right) \\ -\frac{L^2 + 2R^2}{\left(L^2 + 4R^2\right)^{\frac{1}{2}}}\tan^{-1}\left[\frac{X\left(L^2 + 4R^2\right)^{\frac{1}{2}}}{L}\right] \end{array}\right\}, \tag{13}$$

where $R = \frac{r_1}{r_2}$; $L = \frac{l}{r_1}$; $X = (R^2 - 1)^{\frac{1}{2}}$.

5. MATLAB Script

A radiation enclosure involves two surfaces that communicate via thermal radiation or conduction. The first step in using the MATLAB script is to define the radiation enclosure of interest within the model. This is done by inputting a series of matrices corresponding to the characteristics of the inner and outer geometry, best

described by an example of a domed pressure vessel located at a certain height inside a containment of constant radius such as those shown in Fig. 3 and Fig. 7.

The first set of discretizations is from the base of the containment to the bottom of the pressure vessel. The second set covers the range of the increasing-radius, domed-region of the pressure vessel to where the pressure vessel becomes a constant-radius cylinder. The third set covers the height of this cylindrical pressure vessel to where the top dome begins. The fourth set of discretizations is this decreasing-radius, domed-region of the pressure vessel. The fifth and final region is the space from the top of the pressure vessel to the top of the containment. The script's capabilities cover the following geometries: cylinder, ellipse increasing in radius, and ellipse decreasing in radius. In summary, if the inner or outer geometry changes, this point of change must be noted in MATLAB.

From here, the use of the script branches into two sections: radiation shape factor calculation and hydrodynamic volume-related calculations. The latter discretizes the top and bottom domes of Fig. 13 into a series of stacked cylinders. The radius of the discretized cylinder, r_{cyl}, is based on the maximum radius of the ellipse, r_{max}, the discretized height, h, and the total height, b, as seen in Eq. (14). The half-height, $\frac{h}{2}$, is used to determine the radius of the discretized cylinder to guarantee that a cylinder of zero radius is not input into RELAP.

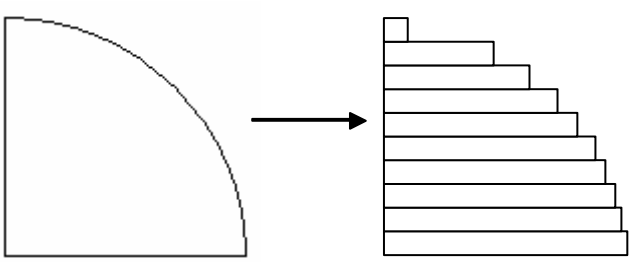

Fig. 13. Discretizing a dome into a series of stacked cylinders.

$$r_{cyl} = r_{\max} * \left\{ 1 - \left[\frac{\left(r_{\max} - \frac{h}{2} \right)}{b} \right]^2 \right\}^{1/2}, \tag{14}$$

The hydrodynamic volumes are defined between the radius of the inner structure and the outer structure. Using the aforementioned method of discretizing the elliptical domes maintains the size and shape of the hydrodynamic volumes in these regions, which benefits the accuracy of the experiment simulation.

The script also moves to improve the accuracy of the experiment simulation by compensating for the limitation in RELAP5-3D's radiation enclosure model that only regards the left and right surfaces of a heat structure. An elliptical domed pressure vessel is shown in part (A) of Fig. 14. Discretizing the elliptical domes into cylinders using Eq. (14) does maintain the volumes and the general shape of the original hydrodynamic volume, but it introduces a problem into radiation shape factor calculation illustrated in Part (B) of Fig. 14. As the radius of the discretized cylinder decreases, the cylinder becomes hidden with respect to its shape factor to and from other nodes. To compensate for this problem, the MATLAB script treats the inner and outer geometries as concentric

cylinders, which is shown in Part (C) of Fig. 14. By flattening the elliptical domes, the script accounts for heat transfer areas lost to the top or bottom of the cylinders discretized by Eq. (14).

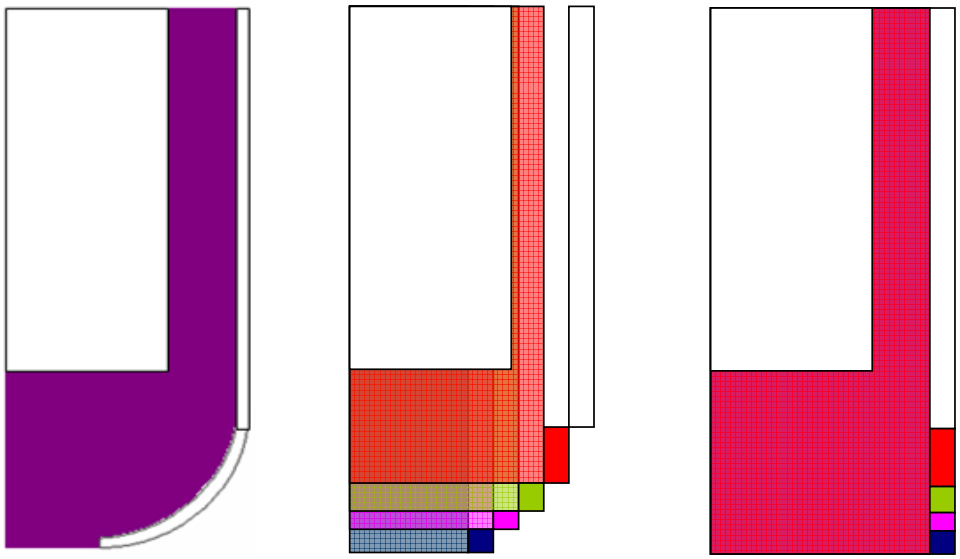

Fig. 14. Comparison of methods to discretize domes.

In the case of the VGM experiment, the script mitigates the effects of modeling the series of vertical cooling tubes as a single outer annulus. Radiation is the predominant heat transfer mode from the pressure vessel to the RCCS. Therefore, the script places the annulus at a certain radius to ensure that the fraction of thermal energy that reaches the annulus from the pressure vessel is the same as the fraction that reaches the cooling tubes from the pressure vessel. Following the entry of model dimensions, such as pressure vessel outer diameter and RCCS tube diameter, the MATLAB script discretizes the model into a series of axial cells. The cell height and radii are then input

into correlation C-101 to find the view factor from a single cooling channel to the main body of the reactor vessel. The reciprocity and the summation rule of Eq. (4) and (5) enable the calculation of the view factor from the reactor vessel to all 432 cooling channels. C-92 finds the view factor from the reactor vessel to the inside surface of the outer cylinder.[14] By using the shape factor from the reactor vessel to all of the cooling channels in the equations of C-92, the radius of the equivalent single outer cylinder is found. This view factor represents the fraction of thermal energy leaving a cell on the reactor vessel and striking its counterpart directly across on the outer cylinder. It is important to note that facing heat structure cells must be of equal height. As yet, there has been no consideration for the radiant effects of a reactor vessel cell on adjacent outer cells, those at either side of the counterpart on the outer cylinder seen in Fig. 15.

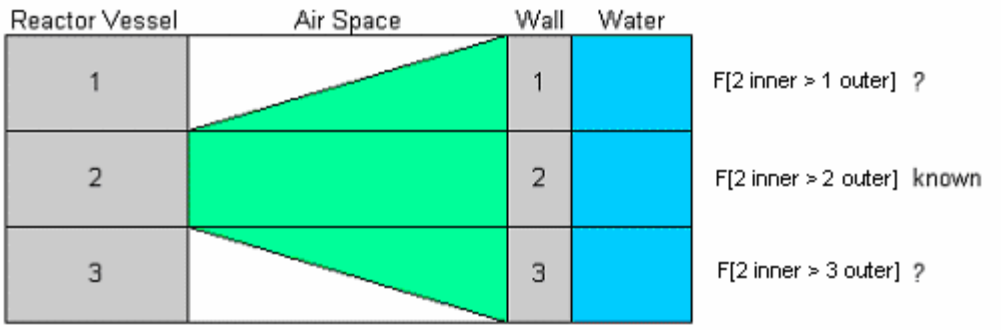

Fig. 15. Cell 2, sample view factor calculation.

The C-95 correlation is used to find the view factors to these adjacent cells and to cells further away, i.e. imaginary cells 4, 5, and 6 on Fig. 15. The MATLAB script performs these calculations for each cell on the reactor vessel, creating an array of view factors. Then, by the reciprocity relation of Eq. (4), the view factors from the outer wall to the reactor vessel are found. The effect of employing the C-95 correlation over simply

using the straight-across view factors is analyzed for the VGM case, which is less complex than the HTTR case.

The script then calls the B-55 correlation to find the view factors from elements on the outer cylinder to other elements on the outer cylinder, $F_{2\_outer\text{-}1\_outer}$ and $F_{2\_outer\text{-}3\_outer}$ for example. The equations of B-55 are limited to regions where the interior cylinder is of constant radius. Such regions are maximized when the experiment geometry is modeled as concentric cylinders, which is the case for radiation shape factor calculation.

After employing the listed correlations, however, the summation rule of Eq. (5) will not be satisfied, meaning that the sum of all the view factors will likely not equal 1.0. This mismatch arises because the enclosure is not modeled as being capped and the cylinders are not of infinite length. Therefore, the remaining view factor is added to $F_{i\text{-}i}$, the fraction that the cell transmits to itself, which satisfies both the reciprocity and the summation conditions of Eq. (4) and (5). The MATLAB script then formats and otherwise prepares this information for the RELAP input deck.

B. VGM Model

With the aid of the MATLAB script, the RELAP5-3D input deck is created to establish a base input deck from which sensitivity studies are conducted. The nodalization of the VGM reactor in the base input deck is shown in Fig. 16.

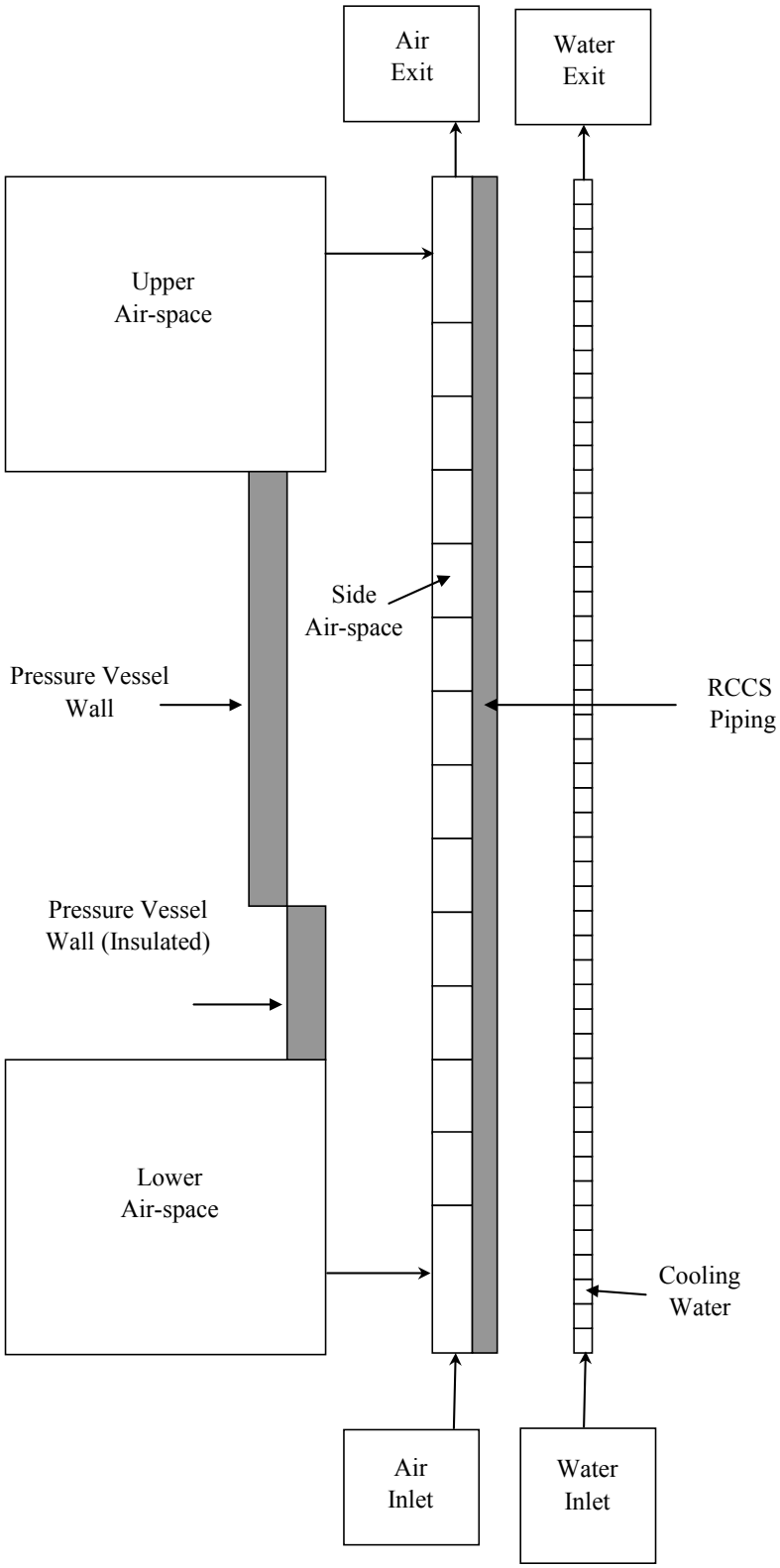

Fig. 16. VGM nodalization.

The model is made of two sets of hydrodynamic volumes: an air-space and a water-space. The air-space, containing air at ambient conditions (25 ^{o}C, 1 bar) is subdivided into three regions: a lower region, a side region, and an upper region. This subdivision is necessary to satisfy the node length-to-diameter ratio requirement. The upper and lower regions are comprised of one node each, while the side region is comprised of 14 axial regions. Single junction components connect the lower region to the side region and the upper region to the side region. A time-dependent volume connects to the lowermost volume of the side air-space and another to the uppermost volume to provide a source and a dump for to simulate airflow by natural convection through the system. The water-space, which has a much smaller diameter, simulates water in the RCCS and is comprised of 46 axial regions with both inlet and outlet time-dependent volumes. The inlet water temperature and flow rate are dictated by the experiment conditions: 43 ^{o}C and 9.82 kg/s for the pressurized case and 42 ^{o}C and 10.3 kg/s for the depressurized case. Only the inlet water temperature is given. To prevent the water in the tube from flashing to steam, the inlet water pressure is set high at 3 bar. The two hydrodynamic volumes are separated by a heat structure which simulates the RCCS pipe thickness.

The model contains two sets of heat structures, one that simulates the RCCS piping and the other that simulates the pressure vessel. The single radiation enclosure lies between these two sets of heat structures. The stainless steel 20 RCCS piping is 4 mm thick and contains 46 axial nodes. The equivalent outer cylinder obtained by the C-92 shape factor correlation acts as the RCCS. The right face of this heat structure is bounded by the water and has a heat transfer hydraulic diameter of 57 mm, the diameter

of a cooling tube. The left face of the RCCS heat structure is bounded by the air space. The shape factor determination treats both the RCCS and pressure vessel as cylinders of constant radii to compensate for heat transfer area lost in the discretization process. Keeping with this theme, the heat transfer hydraulic diameter for the left face of the RCCS heat structure is based on the cylinders of constant radii. The pressure vessel is divided into four areas: the lower elliptical dome, the main body, the flange, and the upper elliptical dome. The MATLAB script discretizes each section of the pressure vessel for a total of 40 heat structures.

The benchmark problem lists thermal conductivity data for the following materials: St20, St15X12HMCDA, and insulation.[7] Specific heat capacity data is not included within the benchmark problem. Therefore, the cooling tubes, made from St20, are assumed to have the same specific heat capacity characteristics as plain carbon. In St15X12HMCDA, the St15 designates manganese content from 1.00% to 1.65% so this material is treated as having the same specific heat capacity characteristics as high-manganese carbon steel, G15240.[14] The insulation surrounding the lower portion of the pressure vessel is given a volumetric heat capacity approximately equal in value to the maximum pressure vessel volumetric heat capacity.

To take full advantage of heat structure to hydrodynamic volume interaction modeling in RELAP5-3D, assignment of the temperature profiles of Fig. 4 to the pressure vessel involves following a standard RELAP5-3D modeling practice. The pressure vessel is made thin-walled and the temperature profiles are assigned to the left surface of the pressure vessel, allowing for conduction through the thin wall to the hydrodynamic volume.

Both the pressurized and depressurized benchmark models are run with and without radiant heat transfer. These different runs are executed to find the convective heat transfer for comparison with the benchmark data that details both radiant and convective heat transfer. Furthermore, the benchmark data shows that radiant heat loss is at least 75% of total thermal energy.[7] Computing convective heat transfer alone, therefore, can be used as another check for the magnitude of radiant heat loss.

C. HTTR Model

The MATLAB script helps to establish a base RELAP5-3D input deck from which sensitivity studies are conducted. The nodalization of the HTTR reactor using discretized domes is shown in Fig. 17 and the nodalization using cylinders of constant radii is shown in Fig. 18.

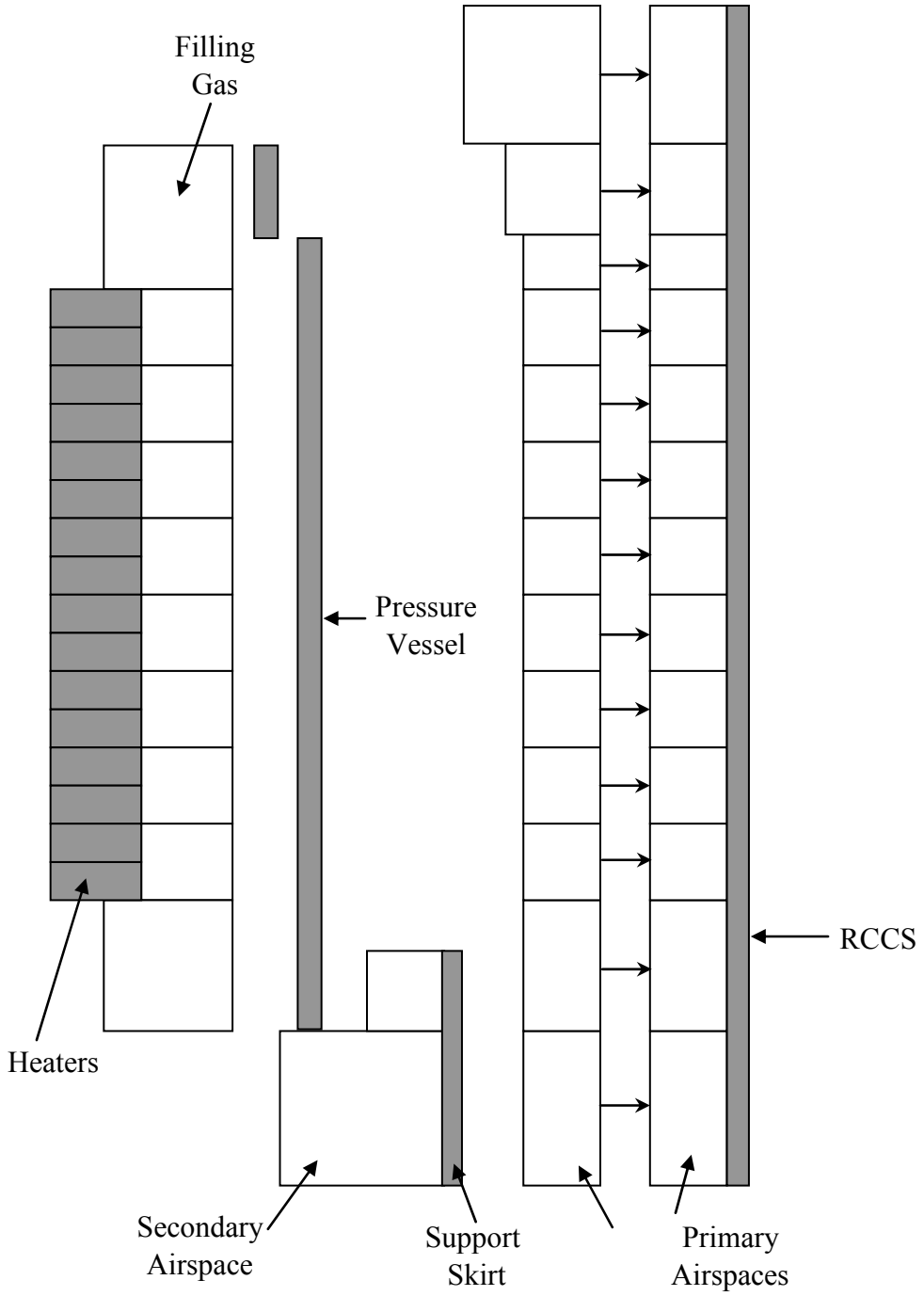

Fig. 17. HTTR nodalization using discretized domes.

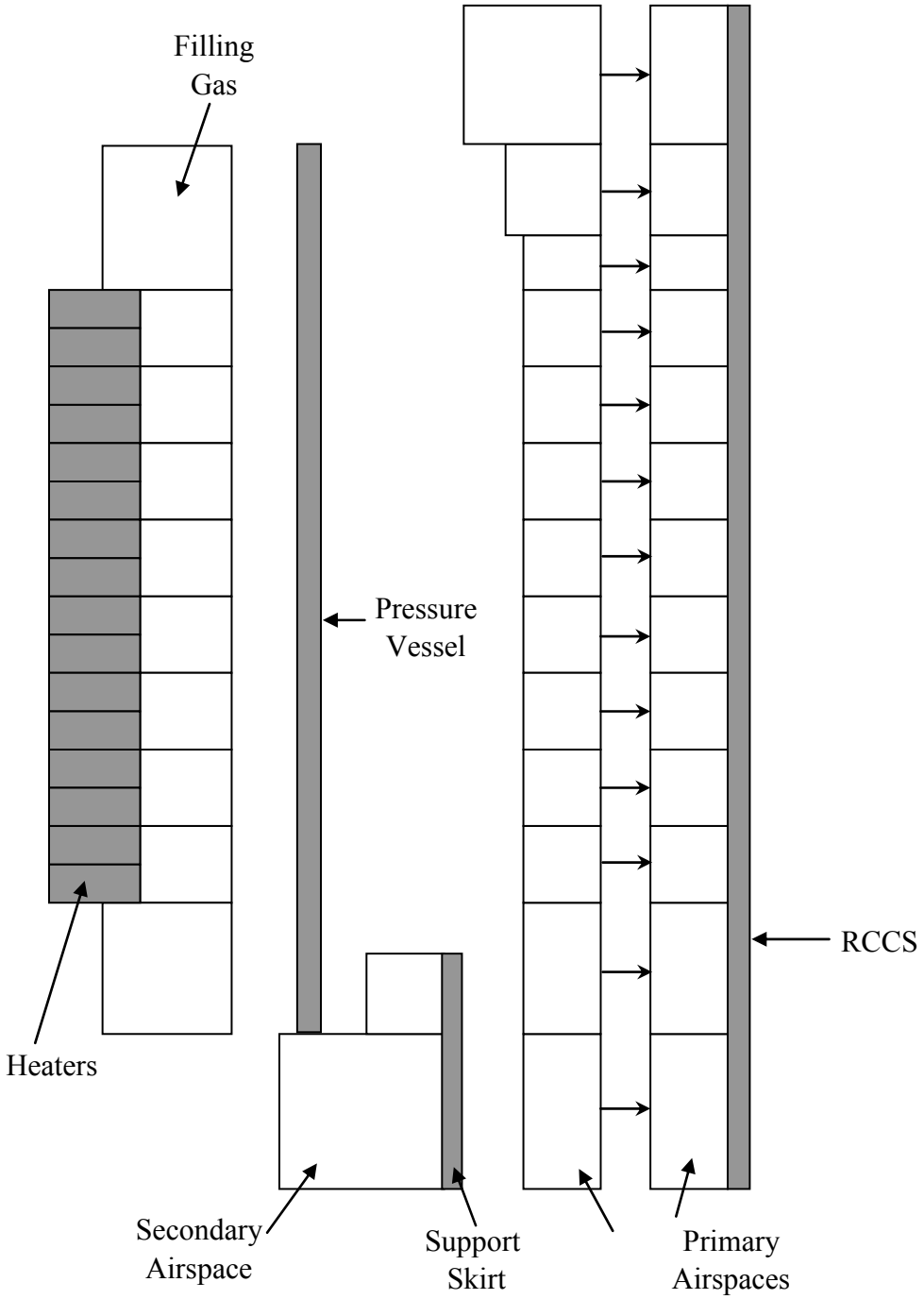

Fig. 18. HTTR nodalization using cylinders of constant radii.

The model contains four sets of heat structures simulating the heating element, the pressure vessel, the pressure vessel supports, and the RCCS piping. One radiation enclosure lies inside the pressure vessel and another outside the pressure vessel. The VGM experiment shows that a single outer cylinder can model the RCCS piping without utilizing the C-92 shape factor correlation to determine the equivalent radius. This single outer cylinder representing the RCCS is comprised of 23 axial nodes. The left face of the RCCS heat structure is bounded by the primary air-space. The right face of this heat structure is bounded by an experiment-specific temperature profile, the temperature measured along the height of the RCCS. Like the VGM model, the temperature profile is assigned to the right face to take full advantage of heat structure to hydrodynamic volume interaction modeling in RELAP5-3D. Similarly, the experiment-specific power profile is assigned to the left face of the thin-walled heating element heat structure.

The heating element heat structure is discretized into 16 equal sections, a number arising from limitations in the modeling technique. The MATLAB script requires that cells straight across from each other in a radiation enclosure have the same cell height. However, RELAP5-3D's radiation enclosure model is limited to 99 cells, implying a maximum of 49 inner cells radiating to 49 outer cells. For a multiple radiation enclosure simulation such as the HTTR, if the heating element-pressure vessel enclosure uses a fine nodalization, then only a limited number of cells can be used in the pressure vessel-RCCS enclosure. Therefore, it is critical to balance the nodalization between the two enclosures. This balance sets the upper bound for the number of nodes that may be used in the heating element-pressure vessel enclosure. The lower bound for the number of nodes in this enclosure is set by adequately capturing the power profile, which acts on the

axial heater segments shown in Fig. 7. Rather than use the total heater height of 2000 mm shown in Fig. 7, the total heater height is based on the heat transfer area of the heating segments shown in Table VI. Heat transfer from the heating segments is assumed to be in the radial direction only. This assumption is reinforced by Table VIII, which calculates an invalid segment height for heater segment number 6 if it transfers heat in both radial and axial directions. Dividing 2.145 m into 16 nodes of equal height balances the number of nodes between the two radiation enclosures while adequately capturing the power profile in most cases. Table IX compares the actual heat segment height with those heights used in the RELAP5-3D input deck and notes that the heat flux from heater 6 is approximately halved. Therefore, to maintain the heat flux defined in the experiment, the power input to heater 6 is doubled. The left face of the heating element heat structure is insulated and the right face is bounded by a hydrodynamic volume filled with experiment-specific gas.

TABLE VIII

Heater segment height calculation from listed heat transfer area

			Heat Transfer	
			Radial Only	Radial and Axial
Heater Radius, m	Heater	Heat Transfer Area, m^2	Segment Height, m	Segment Height, m
0.3	1	0.283	0.150	
	2	0.848	0.450	
	3	0.848	0.450	
	4	0.848	0.450	
	5	0.848	0.450	
	6	0.135	0.072	-0.078
		Total Segment Height (TSH), m	2.021	
		Space, m	0.124	
		TSH + space, m	2.145	

TABLE IX

Heater segment height, actual versus model

	Segment Height, m		Number of Nodes	Consequence
Heater	Actual	Model		
6	0.072	0.134	1	halves heat flux
5	0.450	0.402	3	higher heat flux
4	0.450	0.402	3	"
3	0.450	0.402	3	"
space	0.124	0.268	2	lower heat flux
2	0.450	0.402	3	higher heat flux
1	0.150	0.134	1	"
		Total Nodes	16	

This same hydrodynamic volume acts as the left boundary for the pressure vessel heat structure, with the primary air-space acting at the right boundary. Like the VGM experiment, the pressure vessel is divided into geometry-based regions: the lower elliptical dome, the main body, and the upper elliptical dome. The MATLAB script is first run for the heating element-pressure vessel enclosure to generate discretized radii for the elliptical sections. The thickness of the pressure vessel, 12 mm, is then added to these discretized radii to run the MATLAB script for the pressure vessel-RCCS enclosure. The lower elliptical dome uses one node while the upper elliptical dome uses two nodes. This manner of discretization extends the main body of the pressure vessel by one node at the top and at the bottom for a total of 19 nodes. The second node for the upper ellipse is placed into an additional heat structure located at the top of the pressure vessel.

The cylindrical support skirt surrounding the base of the pressure vessel is divided into three axial nodes. The support skirt is bounded on the left face by the secondary air-space and on the right face by the primary air-space. The HTTR model has three void-spaces, as shown in Fig. 7, but the analysis only uses two radiation enclosures because

the method of modeling prevents shape factor calculation in the cavity below the reactor pressure vessel. Examining the benchmark results for other codes shows that there is a negligible radiant heat transfer through this bottom cavity, which accommodates this modeling technique.[7]

The RELAP3-3D model consists of three sets of hydrodynamic volumes representing gas inside the pressure vessel, air beneath the pressure vessel, and air between the pressure vessel and the RCCS. While the gas inside the pressure vessel varies with the experiment, the two air-spaces are assumed to contain air at ambient conditions. The primary air-space, between the pressure vessel and the RCCS, is subdivided into two regions: an inner and an outer region. This subdivision is necessary to satisfy the node length-to-diameter ratio requirement. Both inner and outer regions are comprised of 13 axial nodes each. Single junction components connect each inner-space node with its outer-space counterpart. For example, an inner-space node at a specific height is connected to an outer-space node at that same height. The secondary air-space, beneath the pressure vessel, is comprised of only two nodes to satisfy the node length-to-diameter ratio requirement. The primary and secondary air-spaces are treated as isolated, having no inlet flow or outlet flow, based on experimental results showing flow fields.[7] The temperature of the filling gas is not given in the benchmark report or in the analyses conducted using other codes, so a range of temperatures are tested.

The benchmark problem lists thermal conductivity data for the following materials: stainless steel (SUS304), carbon steel (C-Mn-Si), plain carbon steel, and ceramics.[7] Specific heat capacity data is not included within the benchmark problem. High-manganese carbon steel, which comprised the pressure vessel in the VGM

experiment, is assumed to comprise the cooling tubes in the HTTR experiment.[16] Stainless steel (SUS304) is assumed to have the same heat capacity characteristics as stainless steel type 304.[16] Although the benchmark report describes the heating elements as being annular ceramic blocks surrounded by nichrome helical coils, insufficient information is given about the dimensions of the coils and the inner region of the ceramic blocks. Therefore, the heaters are modeled as solid alumina (Al_2O_3) ceramic blocks.[17] The benchmark problem lists emissivities for the heat structures but other code analyses predominately use emissivities of Table X.

TABLE X

Heat structure emissivity values

Component	Emissivity
Ceramic heaters	0.93
Pressure vessel	
inner	0.79
outer	0.95
RCCS wall	0.95
Support skirt	0.95

VI. RESULTS

A. *VGM Model*

Using the pressure vessel temperature profile and water conditions prescribed for the pressurized conditions, the RELAP5-3D model presented in the previous chapter is run to steady state. Table XI compares results between RELAP5-3D and the codes used in the benchmark.

TABLE XI

Comparison of calculated heat loss to RCCS for both cases

Pressurized	Total Q, MW	Q-Radiant		Q-Convective	
		MW	% Total	MW	% Total
China (Thermix)	1.22	1.01	83%	0.21	17%
	1.11	1.01	91%	0.10	9%
	1.10	1.01	92%	0.09	8%
	1.12	1.01	90%	0.11	10%
ORNL (MORECA)	1.23	1.04	85%	0.19	15%
Russia (SM1 and DUPT)	1.28	1.03	80%	0.25	20%
	1.17	1.00	85%	0.17	15%
RELAP5-3D	1.30	1.04	80%	0.26	20%

Depressurized	Total Q, MW	Q-Radiant		Q-Convective	
		MW	% Total	MW	% Total
China (Thermix)	1.30	1.08	83%	0.22	17%
	1.19	1.08	91%	0.11	9%
	1.18	1.08	92%	0.10	8%
	1.20	1.08	90%	0.12	10%
ORNL (MORECA)	1.33	1.13	85%	0.20	15%
Russia (SM1 and DUPT)	1.36	1.10	81%	0.26	19%
	1.32	1.12	85%	0.20	15%
RELAP5-3D	1.47	1.18	80%	0.29	20%

Table XI shows that radiant heat transfer from the pressure vessel to the RCCS is the primary afterheat removal mode. RELAP5-3D agrees closely with the Russian results in both radiant heat transfer rate and convective heat transfer rate. Qualitatively, there is good agreement between all of the codes in computing radiant heat transfer rate to the RCCS. A larger disparity lies in the computation of convective heat transfer rate, which can be attributed to the use of different models and approximations within each code. The Thermix simulations vary the convective models, adjusting the radiant heat transfer percentage, but the remaining results report a percentage of radiant heat transfer rate that falls between 80% and 85% of total heat transfer rate.

Because radiant heat transfer is the predominant heat transfer mode, a sensitivity study is conducted varying the emissivity of both the pressure vessel and RCCS. Table XII compares the results of these calculations using different emissivities as a function of both total heat transfer rate and radiant heat transfer rate.

TABLE XII

Emissivity sensitivity study using pressurized case

Emissivity	Total Q		Q-Radiant		% Total		
	MW	% Total	MW	% Q-Radiant	China	Russia	ORNL
0.8	1.30	100%	1.04	100%	100%	100%	100%
0.7	1.12	87%	0.86	83%	83%	83%	83%
0.6	0.96	74%	0.71	68%	68%	68%	68%

The percentages reported by China, Russia, and ORNL are listed in the benchmark report as being a percentage of total heat transfer rate. Table XII implies, however, that the reported percentages are actually a percent of radiant heat transfer rate.

Another sensitivity study is conducted to show the impact of using shape factor correlation C-95 with C-92 versus using C-92 alone. The C-95 shape factor correlation incorporates the effects of angular radiant heat transfer whereas the C-92 shape factor correlation regards only those cells that are straight across. Implementing C-95 is more difficult than using C-92 alone. Table XIII shows that using C-92 alone to calculate radiant heat transfer rate constitutes a mere third of radiant heat transfer rate calculated using C-95 with C-92.

TABLE XIII

Shape factor sensitivity study using pressurized case

Shape Factor Correlation	Q-Radiant	
	MW	%
C-95 and C-92	1.04	100%
C-92 alone	0.33	32%

It is important to note that employing shape factor correlation C-101 to calculate the radius of the equivalent outer cylinder had a negligible effect on the calculated radiant heat transfer rate. This means that RCCS tubes located at a radius of 0.5 m from the center of the containment can be replaced by an equivalent outer cylinder at 0.5 m.

B. HTTR Model

1. Experiment 3

This experiment uses nitrogen at 1.1 MPa as the filling gas. Measured temperatures from the experiment are shown in Fig. 19. The benchmark report does not list a nitrogen temperature, so nitrogen temperature is varied between 150 K and 298.15

K. At this pressure, nitrogen has a critical temperature of approximately 105.24 K, well below the testing temperatures.[18] During the simulation, RELAP5-3D conducts an internal verification to ensure that a noncondensable gas, nitrogen in this case, does not cool below its critical temperature. The results of the RELAP5-3D simulation using the aforementioned nitrogen temperatures are displayed in Fig. 20, treating the pressure vessel as a cylinder in one case and as a more representative discretized shape in another.

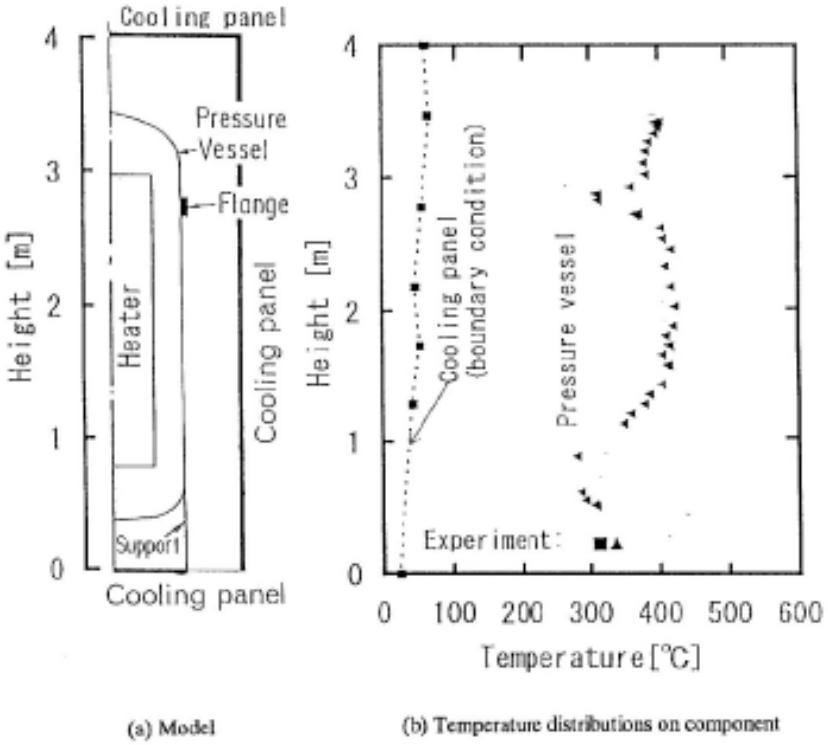

Fig. 19. Experimental results for benchmark problem 3.[7]

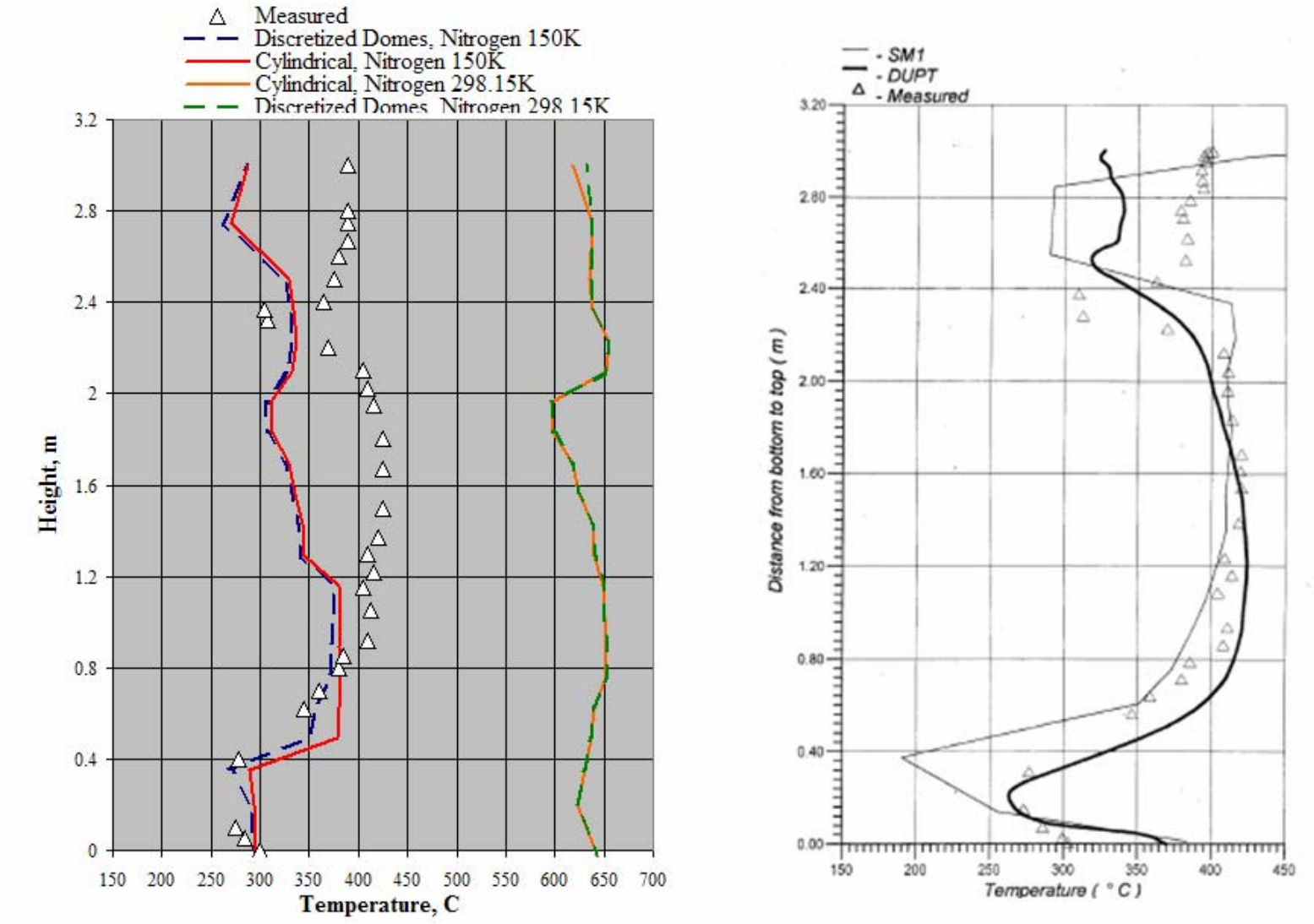

Fig. 20. Experiment 3 simulation, pressure vessel outer surface temperatures.[7]

As Fig. 20 shows, a discretized geometry yields slightly lower pressure vessel outer surface temperatures than a cylindrical geometry, particularly in the lower temperature case. The MATLAB script satisfies the summation rule of Eq. (5) by placing the remaining fraction into how a cell sees itself. The discretized geometry limits the correlations that may be used, which, as in the case of shape factor correlation C-95, are restricted to regions of constant radii. Therefore, in the discretized geometry, particularly in the domed regions, the cell radiates a larger fraction to itself. In contrast, the cylindrical geometry is suited to the application of the shape factor correlations, allowing the cell to primarily radiate to other cells.

Quantitatively, RELAP5-3D predictions vary with boundary conditions. Filling gas temperature has been varied as seen in Fig. 20, but numerous material properties such as volumetric specific heat and emissivity have been assumed also. Qualitatively, RELAP5-3D's temperature trend predictions agree with other computational measurements, such as SM1 and DUPT, as seen in Fig. 20. The height of the space between heaters 2 and 3 is doubled in the RELAP5-3D model, accounting for the temperature loss at around 2 m. A comparison between code predictions and experimental measurements shows good agreement over the main part of the pressure vessel. Towards the top and bottom of the curved pressure vessel, however, the codes fail to fully capture the phenomenology of the experiment, resulting in higher discrepancies between code and experiment. These differences arise from the codes being system analysis codes rather than computational fluid dynamics codes.

Codes reporting results to this benchmark experiment analyzed only a select few of the listed experiments. Most of the codes simulated Experiment 3, however, so, for

comparison purposes, this experiment is chosen as the base model for sensitivity studies.. The first sensitivity study examines the effect of changing the overall nodalization. This study compares the cylindrical predictions of Fig. 20 with a model that uses a single rather than split air space, with a much finer nodalization in the top and bottom regions. In fact, the hydrodynamic cells of this new model fall below the length-to-diameter restriction. Some important differences between the models are that the split air space model includes a support skirt whereas the high discretization model does not. Furthermore, the high discretization model required a much higher air temperature to achieve this agreement. Despite these differences, it is interesting to note the curve trends, seen in Fig. 21.

Splitting the air space improves the ability of the RELAP5-3D code to capture the temperature trends in the top and bottom regions. However, splitting the air space requires more volumes, more junctions between these volumes, and a finer time step to avoid a thermodynamic property error. The resultant increase in computation time is not warranted beyond a certain point because the system analysis code will never fully capture the phenomenology around the domes of the pressure vessel.

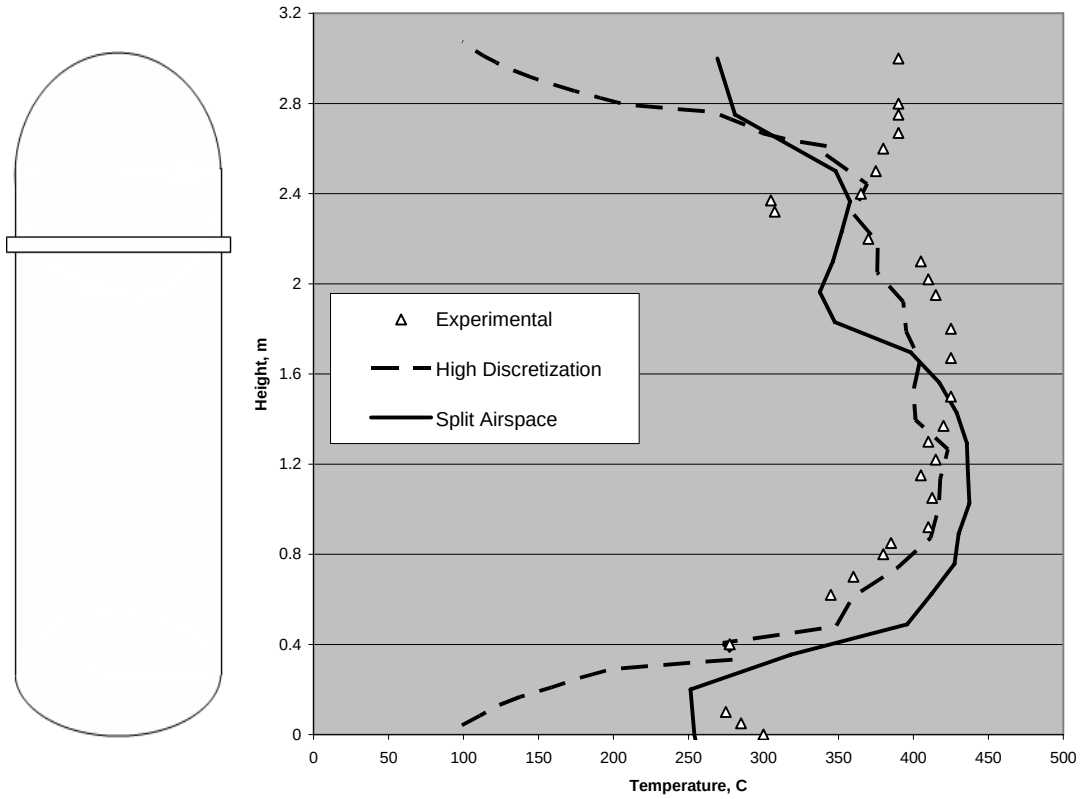

Fig. 21. Model sensitivity to nodalization.

Comparing the heater schematic of Fig. 7 to the experimental temperature measurements of Fig. 19, it appears from the measured temperature dip around 2.4 m that the space between heaters 2 and 3 may actually lie between heaters 1 and 2. The results of a simulation testing this theory are shown in Fig. 22, which shows an improvement in the temperature trend prediction after the space is moved from between heaters 2 and 3 to between heaters 1 and 2.

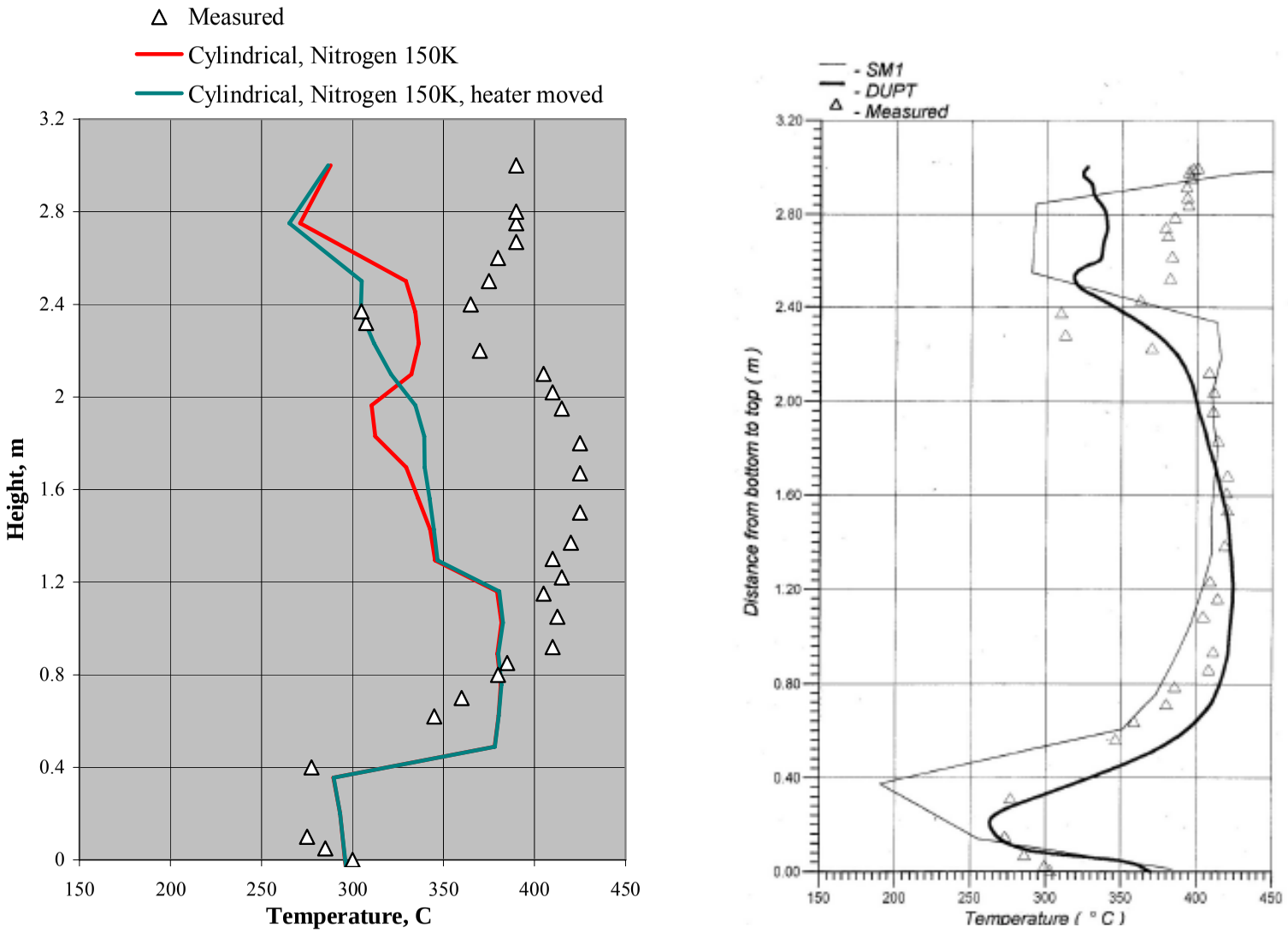

Fig. 22. Experiment 3 simulation, effect of moving space between heaters.[7]

2. Experiment 2

This experiment uses helium at 0.73 MPa as the filling gas. Measured temperatures from the experiment are shown in Fig. 23. The benchmark report does not list a helium temperature, so helium temperature is varied between 50 K and 100 K. At this pressure, helium has a critical temperature less than 9 K, below the testing temperatures. In addition to varying the temperatures, the effect of moving the heater space is tested. Only the shape factor calculation for the cylindrical geometry is considered. The results of the RELAP5-3D simulation using the aforementioned helium temperatures and heater configurations are displayed in Fig. 24.

From Fig. 24, as in Experiment 3, a large discrepancy lies in quantitative temperature predictions between RELAP5-3D and the other codes. Qualitatively, however, the temperature trend prediction for helium at 100 K more closely matches the predictions of other codes than for helium at 50 K. Moving the heater produces slightly higher temperatures as seen in the 50 K case. Again, at the top and bottom of the pressure vessel, the code fails to fully capture the phenomenology of the experiment.

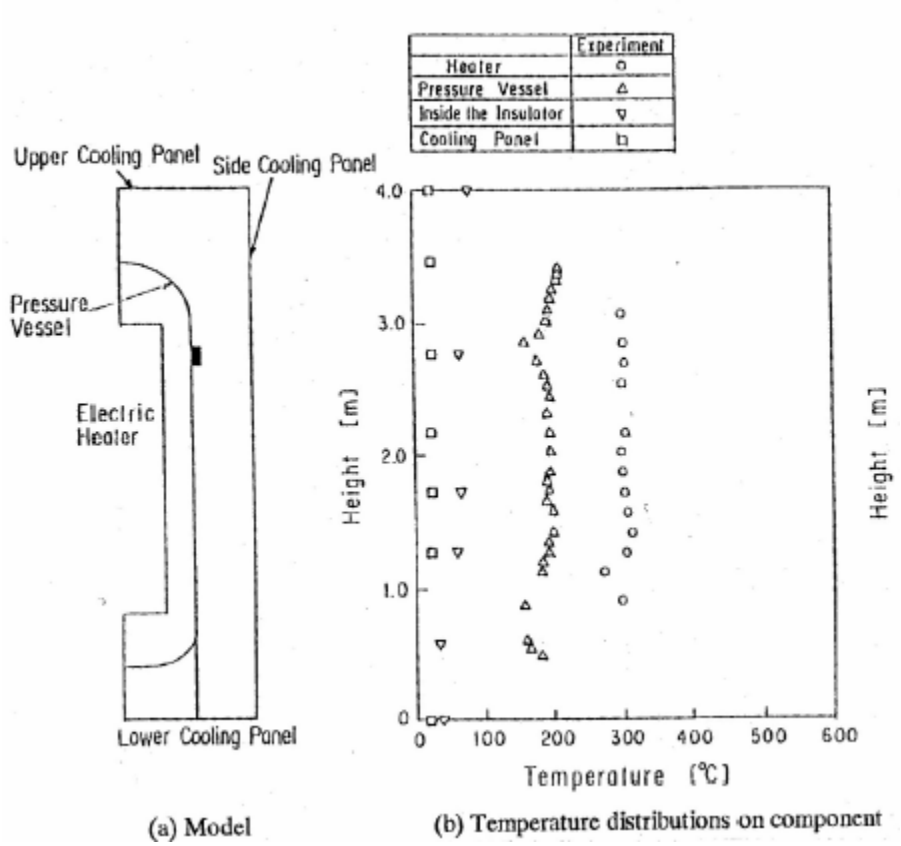

Fig. 23. Experimental results for benchmark problem 2.[7]

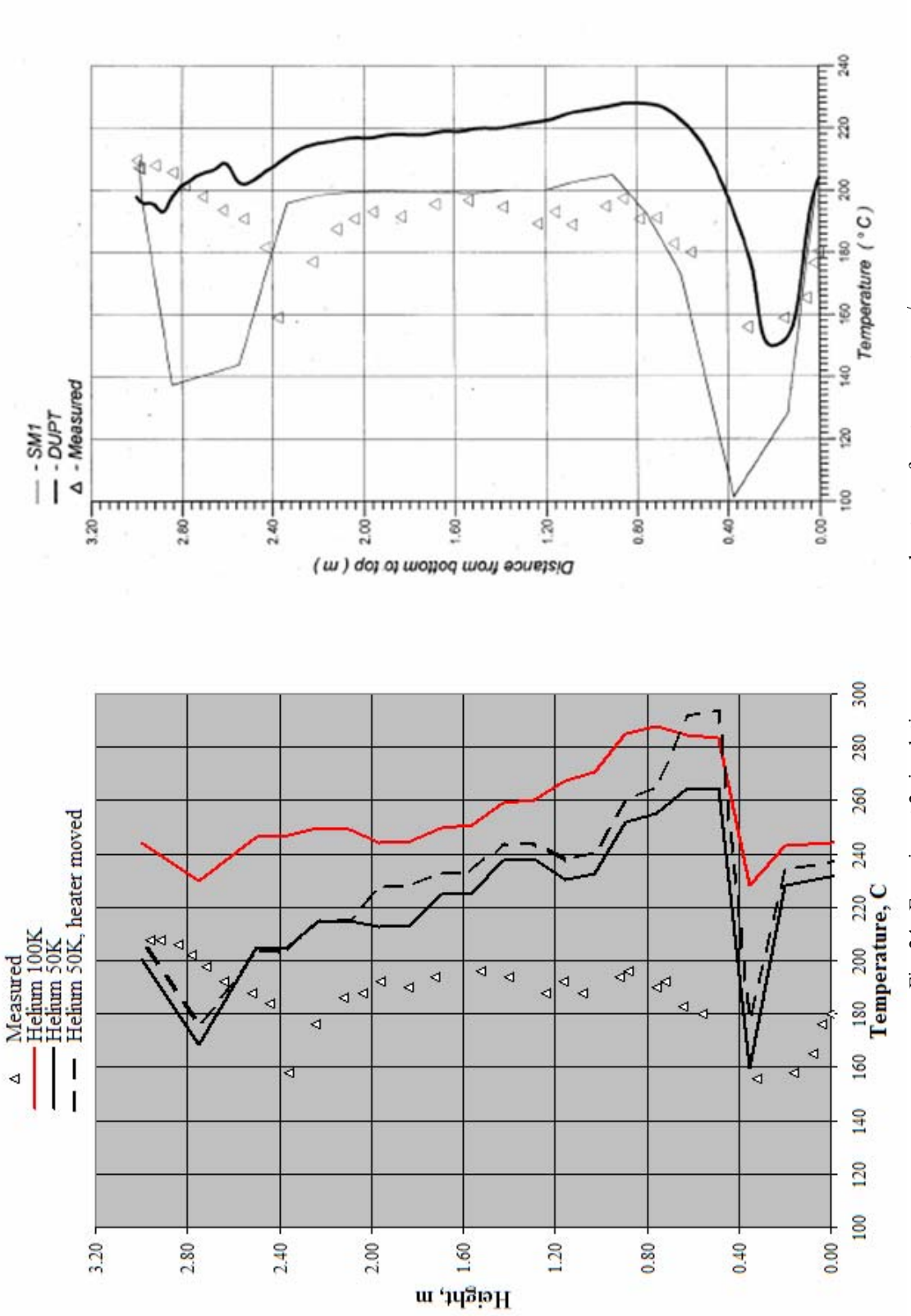

Fig. 24. Experiment 2 simulation, pressure vessel outer surface temperatures.

3. Experiment 4

This experiment uses helium at 0.47 MPa as the filling gas. Measured temperatures from the experiment are shown in Fig. 25. The benchmark report does not list a helium temperature, but learning from Experiment 2, a helium temperature of 100 K is tested. At this pressure, helium has a critical temperature less than 9 K, below the testing temperature. The effect of moving the heater space is tested, but only the shape factor calculation for the cylindrical geometry is considered. This experiment includes standpipes, which act to prevent both convective and radiant heat transfer through the top of the pressure vessel. The outer radius of the standpipes is not explicitly stated, so a cylinder radius of 0.312 m is assumed. As shown in Fig. 25, this cylinder extends from the top of the pressure vessel to the ceiling of the containment. The results of the RELAP5-3D simulation using the aforementioned helium temperatures and heater configurations are displayed in Fig. 26.

From Fig. 26, as in Experiment 3, a large discrepancy lies in quantitative temperature predictions between RELAP5-3D and the other codes. Qualitatively, however, the temperature trend prediction for helium at 100 K closely matches the predictions of other codes. Moving the heater produces slightly higher temperatures and improves the temperature trend prediction. The presence of standpipes improves agreement between code predictions and experimental measurements because the volume above the pressure vessel is reduced.

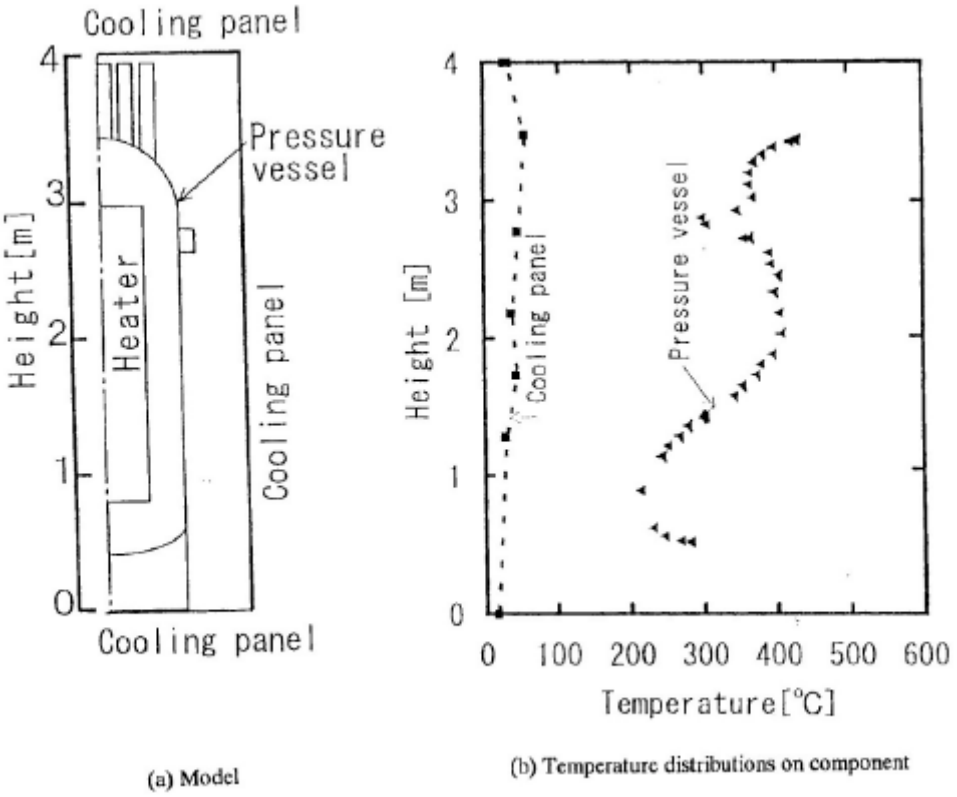

(a) Model

(b) Temperature distributions on component

Fig. 25. Experimental results for benchmark problem 4.[7]

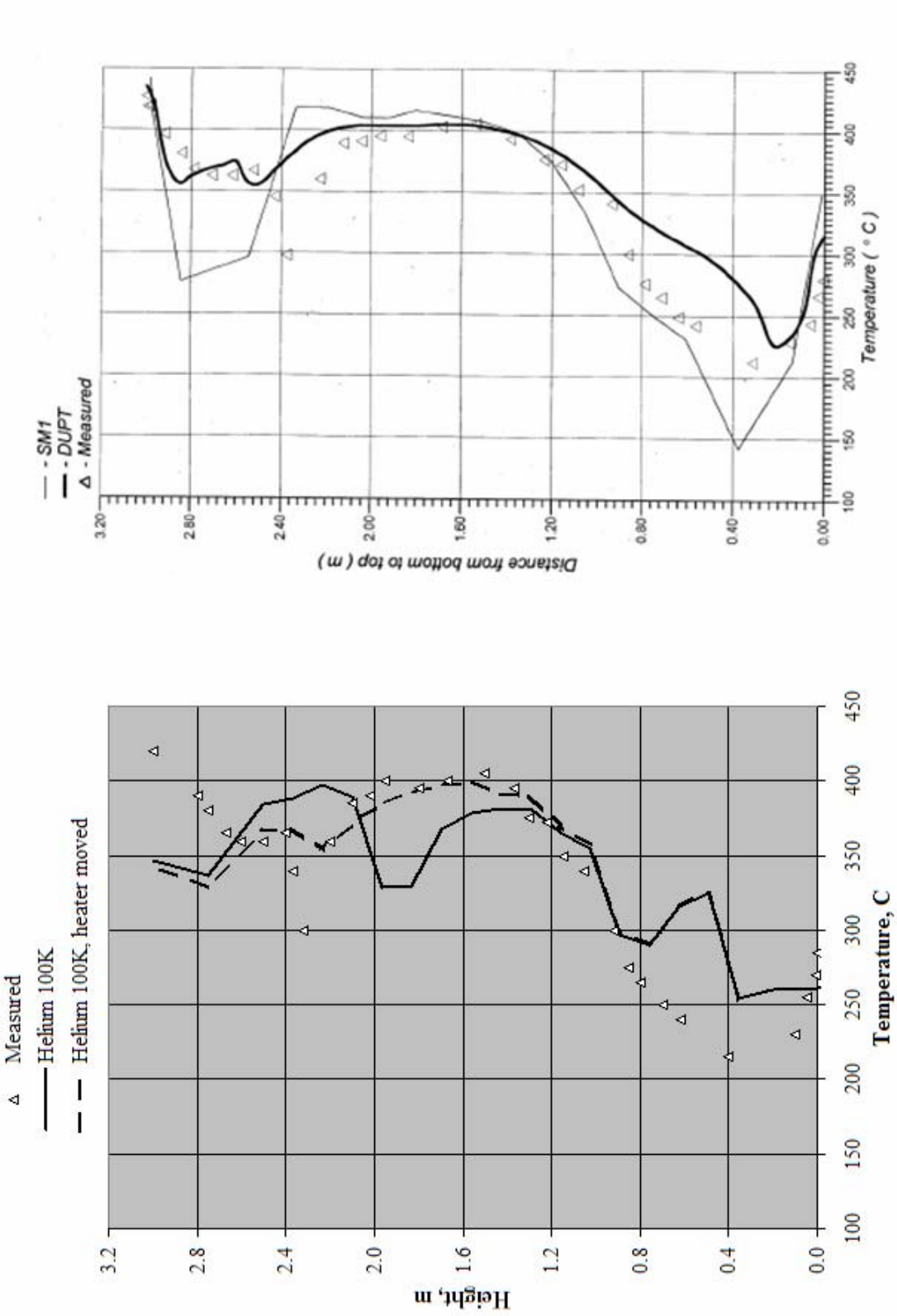

Fig. 26. Experiment 4 simulation, pressure vessel outer surface temperatures.[7]

VII. CONCLUSIONS

Proven extensively for light water reactors, the basic physical models within RELAP5-3D v2.3.6 need to be tested for HTGR designs through conducting benchmark exercises. Two such exercises have been selected to, first, benchmark RELAP5-3D against other codes and to, second, benchmark RELAP5-3D against experimental measurements.

The first benchmark exercise, a code-to-code experiment, used a model of a Russian VGM reactor plant. Both a pressurized and a depressurized plant condition are tested. Material properties such as volumetric specific heat are not given in the benchmark description and are matched to available data. Qualitatively, RELAP5-3D agrees closely with the other codes regarding the percentage of total heat transfer rate to the RCCS that is radiant or convective. The majority of the codes calculate that radiant heat transfer rate accounts for 80 % of the total heat transfer rate to the RCCS. Quantitatively, for both exercises, RELAP5-3D's predictions of the heat rate to the RCCS water are slightly higher than those predicted using MORECA, SM1, DUPT, and Thermix. The largest discrepancies occur in convective heat transfer rate, which may result from differences in both the type of and the implementation of convection models between codes. Differences in radiation shape factor calculation may lead RELAP5-3D to calculate a higher radiant heat transfer rate. A sensitivity study comparing calculated heat transfer rate using different sets of shape factor correlations shows the significance of using as many adjacent cells as possible.

This sensitivity study is reinforced by a sensitivity study conducted for the HTTR model, which specifically tests different methods of implementing shape factor

correlations. The correlations themselves are limited to regions of constant radii, so the MATLAB script is used for two cases: a discretized geometry and a cylindrical geometry. The discretized geometry refers to a nodalization that is representative of the shape of the model, while the cylindrical geometry tries to maintain the surface area of the model. In the cylindrical case, the pressure vessel can distribute the majority of its radiant energy to other cells. In the discretized case, however, the pressure vessel cells radiate a larger fraction to themselves to satisfy the summation condition of Eq. (5). A greater importance is placed on the trend predictions due to initial conditions and material properties assumptions. For both cases, the temperature trend predictions agree with experimental measurements for the main body of the pressure vessel. Towards the top and bottom of the vessel, in the domed regions, RELAP5-3D cannot fully capture the phenomenology of the experiment. Experiment 4 results reinforce this point as the presence of standpipes, which prevent convective and radiant heat transfer through the top of the vessel, improves code predictions. Refining the nodalization axially in another sensitivity study infringes on the length-to-diameter restriction. Radial refinement requires additional junctions and a significant decrease in the minimum time step used by RELAP5-3D to make such a simulation computationally expensive considering the outcome. With a system analysis code, fully capturing the phenomenology of the domed regions is unlikely. Similar results from other code predictions such as SM1 and DUPT reinforce this notion.

With careful modeling and logical assumptions, RELAP5-3D has success in qualitatively capturing the temperature behavior as shown in the HTTR experiment and agreeing closely with other system analysis codes as shown in the VGM experiment. For

more quantitative agreement and to fully capture the phenomenology of the domed regions, it is recommended that RELAP5-3D be coupled with a computational fluid dynamics code such as Fluent.

REFERENCES

1. P. POHL, "AVR Decommissioning, Achievements and Future Programme," IAEA-TECDOC—1043, International Atomic Energy Agency (1997).
2. M.P. VAN STADEN, "Analysis of Effectiveness of Cavity Cooling System," *Proc. 2nd International Topical Meeting on High Temperature Reactor Technology*, Beijing, China, September 22-24, 2004.
3. A. KOSTER, R. MATZIE, and D. MATZNER, "Pebble-bed modular reactor: a generation IV high-temperature gas-cooled reactor," *Proc. I MECH E Part A Journal of Power and Energy*, 218, 309-318 (2004).
4. INTERNATIONAL ATOMIC ENERGY AGENCY, "Considerations in the development of safety requirements for innovative reactors; Application to modular high temperature gas cooled reactors," IAEA-TECDOC—1366 (2003).
5. P.E. MACDONALD, "Next Generation Nuclear Plant (NGNP) A Very High Temperature Gas-cooled Reactor (VHTR)," *Proc. Advanced Reactor, Fuel Cycle, and Energy Products Workshop for Universities*, Gaithersburg, Maryland, March 4-5, 2004.
6. A.G. BAYDAKOV, N.G. KODOCHIGOV, N.G. KUZAVKOV, and V.E. VORONTSOV, "GT-MHR as economical highly efficient inherently safe modular gas cooled reactor for electric power generation," IAEA-TECDOC—1210, International Atomic Energy Agency (1998).
7. INTERNATIONAL ATOMIC ENERGY AGENCY , "Heat Transport and Afterheat Removal for Gas Cooled Reactors Under Accident Conditions," IAEA-TECDOC—1163 (2000).
8. D.A. DILLING, S.K. GHOSE, J.M. BERKOE, S.A. CASPERSSON, and G.C. BRAMBLETT, "Passive Decay and Residual Heat Removal in the MHTGR," IAEA-TECDOC—757, International Atomic Energy Agency (1992).
9. V.F. GOLOVKO, A.I. KIRYUSHIN, N.G. KODOCHIGOV, and N.G. KUZAVKOV, "State of HTGR development in Russia," IAEA-TECDOC—899, International Atomic Energy Agency (1995).
10. T. TAKEDA, S. NAKAGAWA, F. HONMA, E. TAKADA, and N. FUJIMOTO, "Safety Shutdown of the High Temperature Engineering Test Reactor during Loss of Off-site Electric Power Simulation Test," *Nuclear Science and Technology*, **39**, 986-995 (2002).
11. S. SHIOZAWA, "Present Status of the High Temperature Engineering Test Reactor (HTTR)," available on the internet at <http://tauon.nuc.berkeley.edu/asia/2000/Shiozawa1.pdf> (Feb. 7, 2006).
12. S. TAKADA, K. SUZUKI, Y. INAGAKI, and Y. MIYAMOTO, "Test apparatus of cooling panel system for MHTGR," IAEA-TECDOC—757, International Atomic Energy Agency (1992).
13. IDAHO NATIONAL LABORATORY, "RELAP5-3D Code Manuals," Revision 2.3, Idaho Falls, Idaho (2005).

14. J. HOWELL, “A Catalog of Radiation Heat Transfer Configuration Factors,” available on the internet at <http://www.me.utexas.edu/~howell/tablecon.html> (Mar. 2, 2006).
15. R. SIEGEL, J. HOWELL, *Thermal Radiation Heat Transfer*, McGraw-Hill Book Company, New York (1972).
16. ASM INTERNATIONAL, “Thermal Properties of Metals,” Materials Park, Ohio (2002).
17. CRC PRESS, “CRC Handbook of Chemistry and Physics”, 83rd Edition, New York, New York (2003).
18. NATIONAL INSTITUTE OF STANDARDS, “Thermophysical Properties of Fluid Systems,” available on the internet at < http://webbook.nist.gov/chemistry/fluid/> (Mar. 2, 2006).

VITA

Name: Eugene James Thomas Moore

Address: Department of Nuclear Engineering, Texas A&M University, 3133 TAMU, College Station, TX 77843-3133

Email Address: dunamase@tamu.edu

Education: B.S., Mechanical Engineering, The Ohio State University, 2002
M.S., Nuclear Engineering, Texas A&M University, 2006